Article
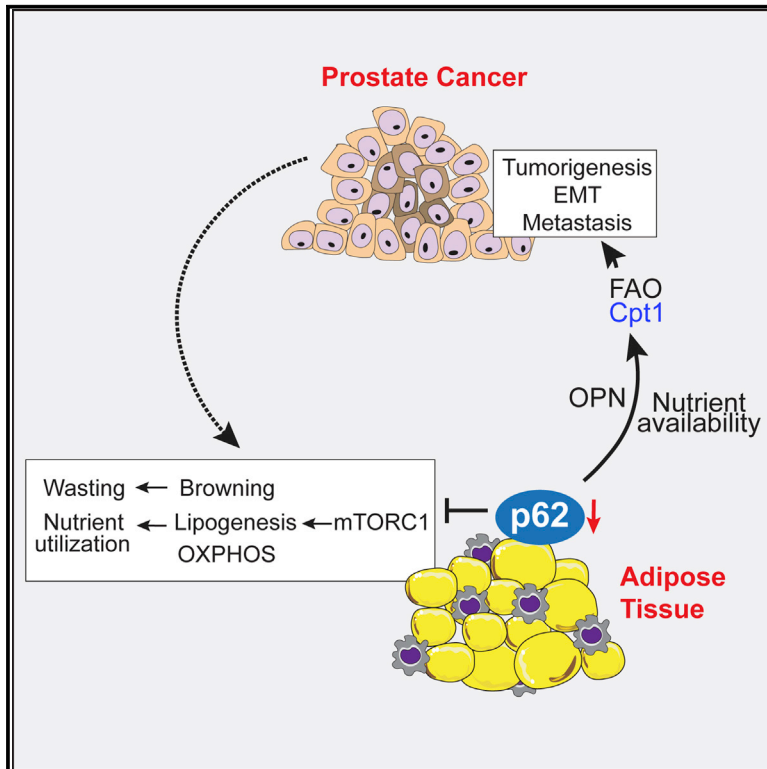
Adipocyte p62/SQSTM1 Suppresses Tumorigenesis through Opposite Regulations of Metabolism in Adipose Tissue and Tumor

Graphical Abstract

Authors

Jianfeng Huang, Angeles Duran, Miguel Reina-Campos, ..., Matthias H. Tschöp, Jorge Moscat, Maria T. Diaz-Meco

Correspondence

jmoscat@sbpdiscovery.org (J.M.), mdmeco@sbpdiscovery.org (M.T.D.-M.)

In Brief

Huang et al. show in a prostate cancer mouse model that p62 loss in adipocytes leads to aggressive disease by increasing osteopontin secretion, which mediates tumor fatty acid oxidation and invasion. P62 deficiency also represses energy-consuming pathways in adipocytes, increasing nutrient availability for tumors.

Highlights

- p62 loss in adipocytes resulted in increased tumorigenesis via secretion of OPN

- p62 inhibition antagonizes tumor-driven energy utilization in the adipose tissue

- Prostate fatty acid oxidation is key for p62-controlled OPN-driven tumorigenesis

- High OPN and CPT1A levels predict poor prognosis in prostate cancer patients

CellPress

Adipocyte p62/SQSTM1 Suppresses Tumorigenesis through Opposite Regulations of Metabolism in Adipose Tissue and Tumor

Jianfeng Huang,[1] Angeles Duran,[1] Miguel Reina-Campos,[1,2] Tania Valencia,[1] Elias A. Castilla,[1] Timo D. Müller,[3,4] Matthias H. Tschöp,[3,4] Jorge Moscat,[1,5,*] and Maria T. Diaz-Meco[1,5,6,*]

[1]Cancer Metabolism and Signaling Networks Program, Sanford Burnham Prebys Medical Discovery Institute, 10901 North Torrey Pines Road, La Jolla, CA 92037, USA
[2]Sanford Burnham Prebys Graduate School of Biomedical Sciences, Sanford Burnham Prebys Medical Discovery Institute, 10901 North Torrey Pines Road, La Jolla, CA 92037, USA
[3]Institute for Diabetes and Obesity, Helmholtz Diabetes Center & German Center for Diabetes Research (DZD), Helmholtz Zentrum München, German Research Center for Environmental Health (GmbH), 85764 Neuherberg, Germany
[4]Division of Metabolic Diseases, Department of Medicine, Technische Universität München, 80333 Munich, Germany
[5]Senior author
[6]Lead Contact
*Correspondence: jmoscat@sbpdiscovery.org (J.M.), mdmeco@sbpdiscovery.org (M.T.D.-M.)
https://doi.org/10.1016/j.ccell.2018.03.001

SUMMARY

Obesity is a leading risk factor for cancer. However, understanding the crosstalk between adipocytes and tumor cells *in vivo*, independently of dietary contributions, is a major gap in the field. Here we used a prostate cancer (PCa) mouse model in which the signaling adaptor p62/Sqstm1 is selectively inactivated in adipocytes. p62 loss in adipocytes results in increased osteopontin secretion, which mediates tumor fatty acid oxidation and invasion, leading to aggressive metastatic PCa *in vivo*. Furthermore, p62 deficiency triggers in adipocytes a general shutdown of energy-utilizing pathways through mTORC1 inhibition, which supports nutrient availability for cancer cells. This reveals a central role of adipocyte's p62 in the symbiotic adipose tissue-tumor collaboration that enables cancer metabolic fitness.

INTRODUCTION

Prostate cancer (PCa) is the second leading cause of cancer death among men in the United States (Brawley, 2012). High prevalence and mortality as well as the long period of time to tumor development are major challenges for PCa research. Obesity is another growing epidemic in Western societies and in developing nations and represents one of the greatest threats to global human health (Finkelstein et al., 2005). Recent epidemiological studies have pointed to an association between obesity and increased risk of cancer, not only in its incidence but also its progression (Calle and Kaaks, 2004). In fact, obesity is the second leading preventable cause of cancer (Wolin et al., 2010),

and given the current obesity epidemic and an aging population, there is increasing concern about the role of obesity in cancer.

There is emerging support for a positive association between obesity and increased risk of PCa, with stronger links to more aggressive fatal disease (Wright et al., 2007). Thus, obesity has been found to be a highly significant risk factor for PCa progression and aggressiveness (Freedland and Platz, 2007; MacInnis and English, 2006), with several studies showing more adverse pathological features and higher risk for biochemical recurrence in obese men undergoing radical prostatectomy (Cao and Ma, 2011; Rodriguez et al., 2001). Severely obese men had a 34% higher risk of dying of PCa relative to men of normal weight (Calle et al., 2003). In addition, obesity has also been associated with

Significance

Obesity is a risk factor in cancer and a fundamental health problem due to the current obesity epidemic. However, the precise crosstalk between adipose tissue and tumor cells remains poorly understood. The adaptor p62 was reported to play an important role in cancers, in both the tumor epithelia and stromal fibroblasts. However, whether it also controls the interactions between tumor cells and adipocytes was unknown, but is an important question for the identification of key metabolic vulnerabilities in this process. Here we establish the role of p62 as a tumor suppressor due to its ability to repress the pro-tumorigenic effects of increased adiposity. Therefore, adipocyte's p62-derived pathways emerge as potential therapeutic targets in the control of tumor-adipose tissue homeostasis.
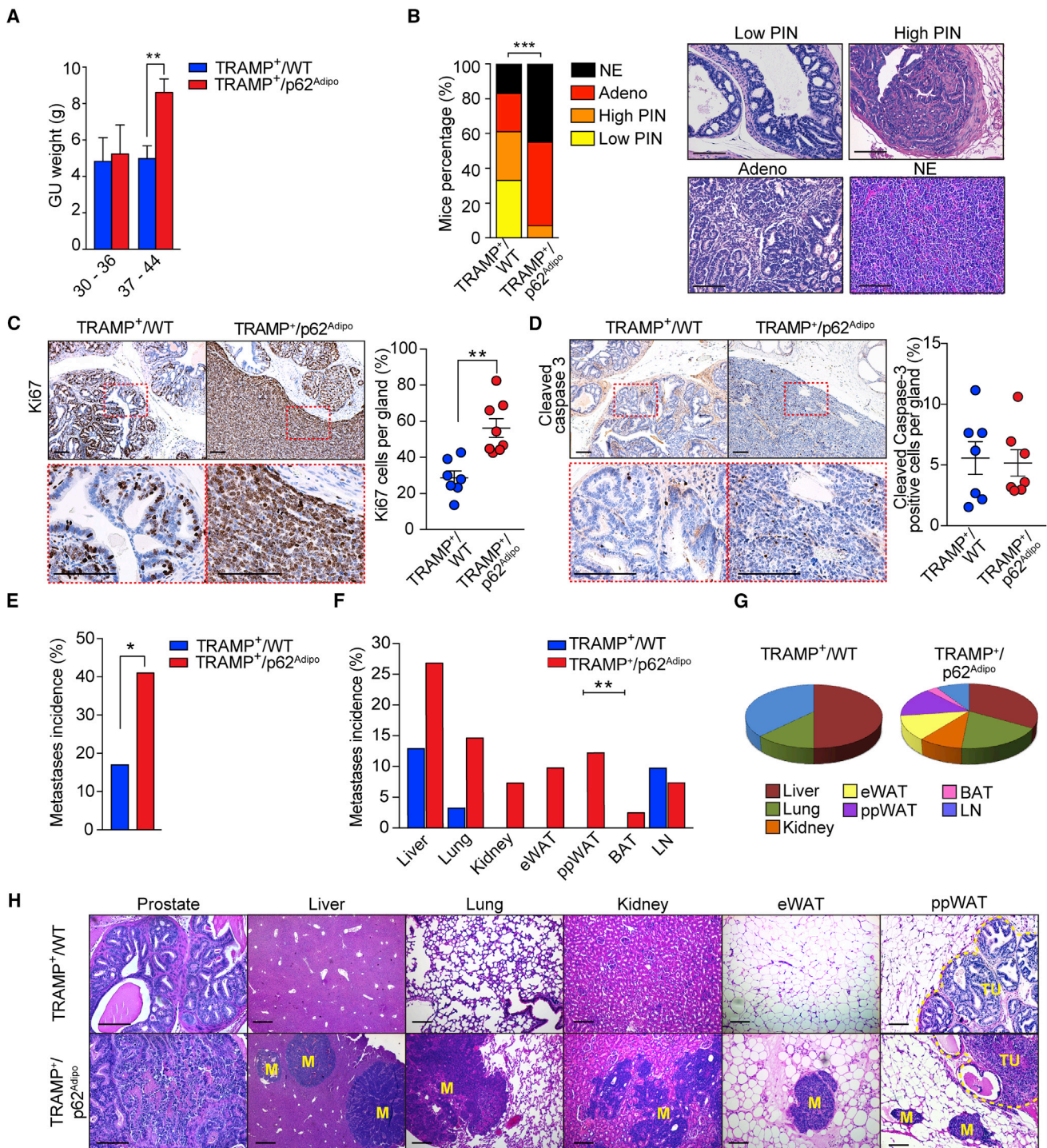
Figure 1. Characterization of PCa Phenotype of TRAMP+/WT and TRAMP+/p62Adipo Mice

(A) Genitourinary tract (GU) weight of 30- to 36-week-old mice (TRAMP+/WT: n = 10; TRAMP+/p62Adipo: n = 8) and 37- to 44-week-old mice (TRAMP+/WT: n = 9; TRAMP+/p62Adipo: n = 22). Student's t test (**p < 0.01).

(B) Frequency of prostatic lesions of different stages in TRAMP+/WT (n = 18) and TRAMP+/p62Adipo mice (n = 29). Right: representative H&E staining of indicated prostatic lesions. Chi-square test (***p < 0.001). PIN, prostatic intraepithelial neoplasia; Adeno, adenocarcinoma; NE, neuroendocrine. Scale bars, 100 μm.

(C and D) Immunohistochemistry (IHC) staining of Ki67 (C) and cleaved caspase-3 (D) and their respective quantification of percentage of positive staining cells per prostate gland in mice at 7–8 months of age (n = 7–8, per genotype). Student's t test (**p < 0.01). Scale bars, 100 μm.

(E) Incidence of metastasis in TRAMP+/WT (n = 31) and TRAMP+/p62Adipo mice (n = 40). Fisher's exact test (*p < 0.05).

increased risk of progression to castration-resistant PCa, the development of metastases, and PCa-specific mortality (Keto et al., 2012). Likewise, higher visceral fat has been shown to be associated with an increased risk for PCa (Finley et al., 2009; von Hafe et al., 2004). However, although epidemiological studies support a role for obesity and weight gain as important risk factors for poor outcome in men diagnosed with PCa, there are still many gaps in our knowledge that need to be investigated to understand the underlying molecular mechanisms of this phenomenon.

Increased adiposity might affect tumorigenesis by providing an excess supply of nutrients and increased levels of pro-inflammatory cytokines, which can be major drivers in different types of cancers, including PCa (De Marzo et al., 2007; Ouchi et al., 2011; Sutcliffe and Platz, 2007). Many studies have addressed the different metabolic wiring of cancer cells under defined cell culture conditions, but very few have considered this from a holistic point of view. In this regard, total body inactivation of the signaling adaptor and autophagy substrate p62 (encoded by the *Sqstm1* gene) results in mature-onset obesity due to increased adiposity and reduced energy expenditure (Rodriguez et al., 2006). Also, the selective genetic inactivation of p62 in adipocytes recapitulates the increased adiposity of total knockout (KO) mice, demonstrating that p62 plays critical roles in repressing adipose tissue expansion (Muller et al., 2013). Importantly, this phenotype is not due to hypothetical differences in locomotor activity or food intake (Rodriguez et al., 2006).

This adipocyte-specific p62 KO model is particularly relevant because most studies addressing the role of obesity in cancer relied on models in which mice are fed a high-fat diet or harbor the genetic inactivation of leptin (Park et al., 2010; Venkateswaran et al., 2007). Both approaches have pleiotropic implications, which complicate the interpretation of the results and do not allow the study of the specific crosstalk between adipocytes and tumor tissue independently of dietary contributions. Here we have addressed this important question by generating mouse lines in which p62 is selectively inactivated, or not, in the adipose tissue in the TRAMP$^+$ mouse model of PCa. This cancer model system is one of the most widely used to investigate prostate tumorigenesis *in vivo* (Greenberg et al., 1995). Using this *in vivo* model and co-culture experiments we investigated the pathways and signaling cascades that govern the crosstalk between adipose tissue and PCa cells, and the role of p62 in that process.

RESULTS

Increased Adiposity Promotes PCa Progression and Metastasis

To establish the molecular mechanisms leading to the crosstalk between the adipose tissue and the tumor in PCa, we sought to establish an endogenous genetic mouse model system in which to carry out cause and effect mechanistic *in vivo* studies independent of food intake and diet. Previously we have identified p62 as a key player in obesity-induced inflammation using an

adipocyte-specific cre system (aP2-Cre). Adipocyte-specific deletion of p62 results in obesity, glucose intolerance, and insulin resistance (Muller et al., 2013). Therefore, we next bred these mice (p62^{Adipo}) with the well-established TRAMP model of PCa to generate TRAMP$^+$/p62^{Adipo} and their corresponding TRAMP$^+$/wild-type (WT) controls. In this model, the oncoprotein, SV40 T antigen (TAg), is expressed under the transcriptional control of the rat probasin promoter, which restricts TAg expression to epithelial cells within the prostate (Greenberg et al., 1995). TRAMP$^+$/p62^{Adipo} mice lack p62 selectively in the adipocytes and develop PCa. To demonstrate the selective deletion of p62 in adipocytes and the lack of hypothetical off-target effects of the aP2-Cre system in macrophages, we doubly stained epididymal WAT (eWAT) from p62^{Adipo} mice for p62 and F4/80, and confirmed the exclusive deletion of p62 in adipocytes (Figure S1A). Also, the macrophages isolated from p62^{Adipo} WAT maintained levels of *Sqstm1* transcripts (coding for p62) similar to those from WT mice (Figure S1B). Furthermore, p62 was not deleted in macrophages in eWAT or periprostatic WAT (ppWAT) from TRAMP$^+$/p62^{Adipo} mice (Figures S1C and S1D).

Although disease-free survival curves (Kaplan-Meier plots) show no differences between both mouse lines, probably due to the large volume of the primary tumor in both groups (not shown), genitourinary (GU) weight was significantly increased in TRAMP$^+$/p62^{Adipo} mice compared with the control group (Figure 1A). Most importantly, we found that TRAMP$^+$/p62^{Adipo} mice developed a more aggressive PCa phenotype with higher incidence of adenocarcinoma and neuroendocrine tumors than TRAMP$^+$/WT controls (Figure 1B). Prostate tumors from TRAMP$^+$/p62^{Adipo} mice displayed increased proliferation, as detected by Ki67 staining (Figure 1C), without differences in apoptosis, as detected by cleaved caspase-3 staining (Figure 1D). TRAMP$^+$/p62^{Adipo} mice also had higher metastasis incidence in liver and lung compared with the control group (Figures 1E–1H). We also found metastasis in kidney, white (WAT), and brown (BAT) adipose tissues in TRAMP$^+$/p62^{Adipo} mice but these were not detected in TRAMP$^+$/WT mice (Figures 1F–1H). Therefore, the selective loss of p62 in the adipose tissue drives tumorigenesis and invasiveness in PCa, which demonstrates, using physiologically relevant genetic *in vivo* models, the existence of a molecular link between the adipose tissue and the tumor.

Adipocyte-Specific p62 Deficiency Modulates the Metabolic Impact of PCa on Adipose Tissue

We next analyzed TRAMP$^+$/WT and TRAMP$^+$/p62^{Adipo} mice from a metabolic point of view by monitoring the body weight of a large cohort of mice for 10 months. Non-tumor-bearing p62^{Adipo} mice display higher body weight, fat mass, and serum triglyceride (TG) levels than p62^{WT} mice, consistent with previous data (Muller et al., 2013). However, in a TRAMP$^+$ background, no differences were observed in any of these parameters between p62^{Adipo} and p62^{WT} mice (Figures 2A–2E). Liver TG and total cholesterol (TC) levels (Figure 2E), and oil red O staining (Figures 2F and 2G) in liver, also revealed no significant differences in lipid

(F and G) Distribution of metastasis sites (F; two-way ANOVA, **p < 0.01) and their corresponding percentages of total incidence (G).

(H) H&E staining of prostates and metastases in different tissues of the indicated genotypes at 37 weeks of age. eWAT, epididymal WAT; ppWAT, periprostatic WAT; TU, tumors; M, metastases. Scale bars, 100 μm.

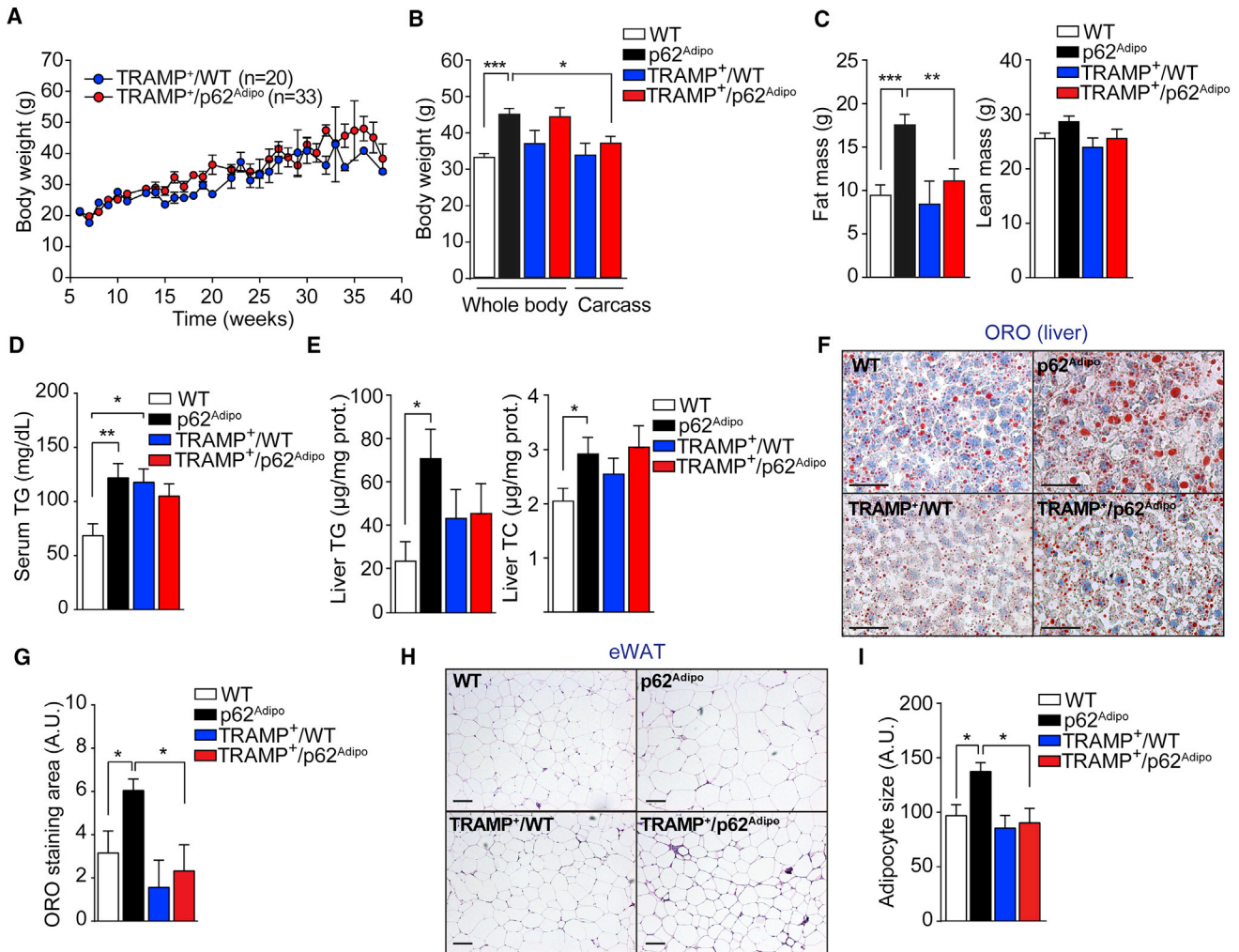Results are presented as mean ± SEM (A, C, D). See also Figure S1.

Figure 2. Metabolic Analysis of TRAMP+/WT and TRAMP+/p62^Adipo Mice

(A) Body weight of TRAMP+/WT (n = 20) and TRAMP+/p62^Adipo (n = 33) mice.

(B) Body weight of WT (n = 19), p62^Adipo (n = 18), TRAMP+/WT (n = 9), and TRAMP+/p62^Adipo (n = 20) at 32–40 weeks of age. Carcass: whole body weight minus GU weight.

(C) Fat (left) and lean (right) mass of 7-month-old mice of indicated genotypes by dual-energy X-ray absorptiometry analysis (n = 5–12, per genotype).

(D) Quantification of serum triglyceride (TG) concentrations of 7-month-old mice (n = 7–12, per genotype).

(E) Quantification of liver TG and total cholesterol (TC) levels of 7-month-old mice (n = 7–10, per genotype).

(F and G) Representative images (F) and quantification (G) of oil red O (ORO) staining in livers of 7-month-old mice (n = 4, per genotype). Scale bars, 100 μm.

(H and I) Representative H&E staining (H) and adipocyte size measurement (I) of eWAT of 7-month-old mice (n = 4, per genotype). Scale bars, 100 μm.

Results are presented as mean ± SEM (A–E, G, I). Student's t test (*p < 0.05, **p < 0.01, ***p < 0.001). See also Figure S2.

accumulation between both genotypes, whereas p62^Adipo mice developed fatty liver in the TRAMP-negative background (Figures 2E–2G). Moreover, the size of adipocytes that was larger in non-tumor-bearing p62^Adipo mice did not differ between both genotypes in TRAMP+ mice (Figures 2H and 2I). These results indicate that the selective loss of p62 in adipocytes results in increased adiposity but this is blunted by the presence of the tumor, which is more aggressive than in p62-proficient mice.

To establish the whole-body metabolic impact of PCa in the context of p62 deficiency on the adipose tissue, we performed a full metabolic characterization of these mice by using an automated indirect calorimetry system (CLAMS). The analysis of all the metabolic parameters measured, including food intake,

drinking, horizontal and vertical activity, volume of O_2 (VO$_2$), volume of CO_2 (VCO$_2$), and respiratory exchange ratio, did not show significant changes between the TRAMP+/p62^Adipo mice group and the control TRAMP+ mice (Figures S2A–S2H). Consistently, energy expenditure did not differ between groups after adjusting for body weight, lean mass, or fat mass according to analysis of covariance (ANCOVA) (Figure S2I). It should be noted that in our previous report of the p62^Adipo mice we showed that they have a reduced metabolic rate caused by impaired non-shivering thermogenesis (Muller et al., 2013). However, the presence of PCa abolished the metabolic differences between WT and p62^Adipo mice. This indicates that the tumor in TRAMP+/p62^Adipo mice increased their metabolic rate. It could be argued that this would
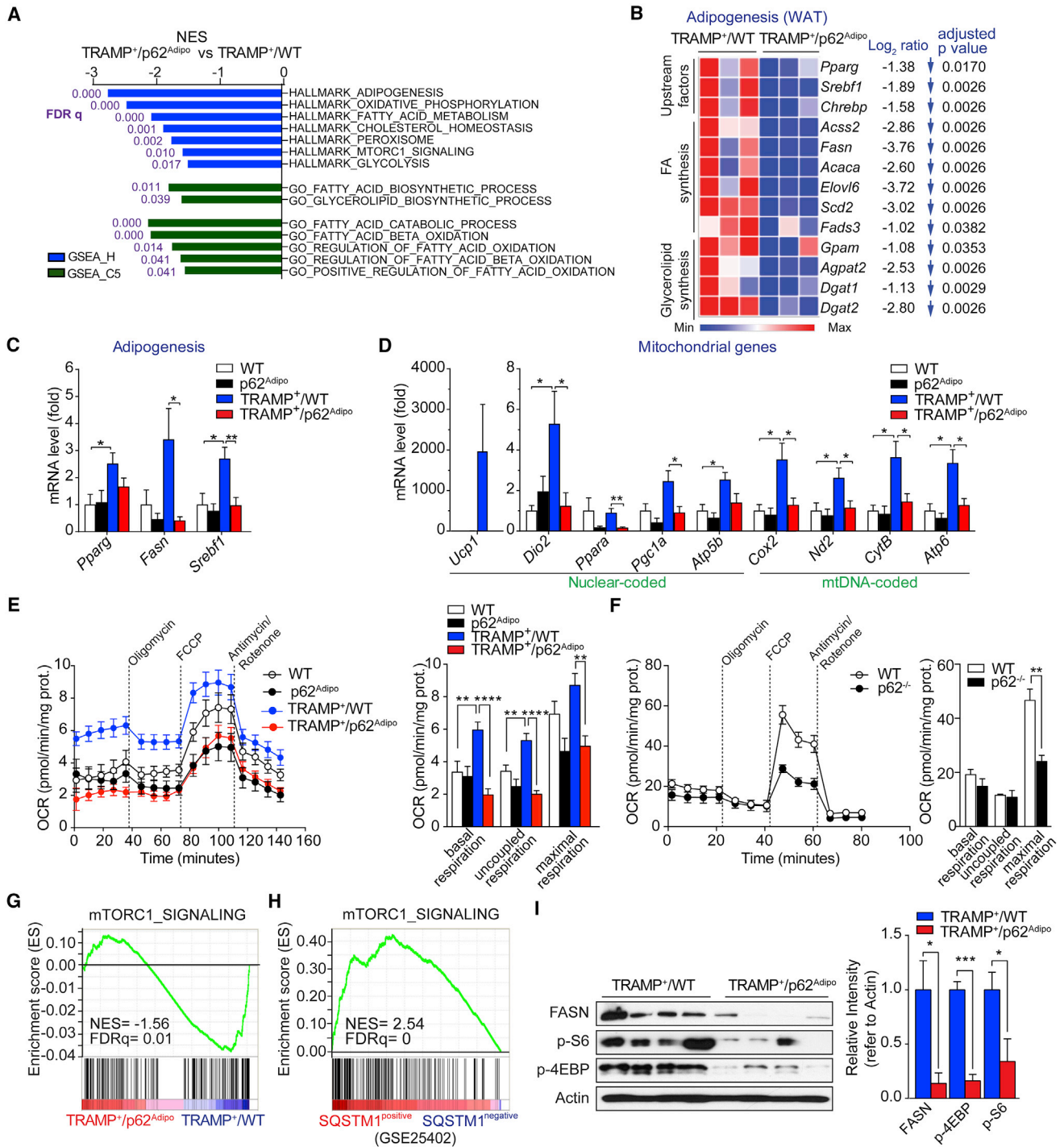
Figure 3. Metabolic Analysis of WAT in TRAMP+/WT and TRAMP+/p62Adipo Mice

(A) Top metabolic pathways from GSEA of downregulated genes in eWAT of TRAMP+/p62Adipo versus TRAMP+/WT mice (n = 3) using GSEA Hallmark and C5_GO biological process MSigDB database.

(B) Heatmap representing the downregulated genes associated with "adipogenesis" in eWAT of mice described in (A).

(C and D) qPCR analysis of adipogenesis-related genes (C) and mitochondrial genes (D) in inguinal (iWAT) of mice of four indicated genotypes (n = 4–6).

(E and F) Oxygen consumption rate (OCR) in iWAT explants (E) from indicated mice (n = 8–10, per genotype) or in primary adipocytes (F) differentiated from WT and p62 KO SVF (n = 3). Left: plot of OCR to time measured by Seahorse. Right: calculated respiration levels of different types.

(G) GSEA plot of enrichment in "mTORC1_SIGNALING" signature in TRAMP+/WT WAT as described in (A).

(legend continued on next page)

be consistent with the increased energy expenditure and activation of thermogenesis that have been proposed as causative of adipose cancer-associated cachexia (Kir and Spiegelman, 2016; Petruzzelli et al., 2014). However, our results shown below demonstrate that this is not the case.

p62 Deficiency Favors Repression of Tumor-Responsive Nutrient-Utilizing Pathways in Adipose Tissue

To understand the mechanisms whereby p62 regulates the pathways that control how adipocytes promote tumorigenesis of PCa, we carried out a genome-wide unbiased approach to analyze gene expression by RNA sequencing in both adipose tissue and PCa tumors. Bioinformatics analysis of the whole transcriptome of WAT from both mouse genotypes revealed, upon deletion of p62, a profound impact on gene expression networks related to metabolism. Thus, gene set enrichment analysis (GSEA) using the curated gene set compilation Hallmark (MSigDb H) of transcripts downregulated in the WAT of TRAMP$^+$/p62^{Adipo} as compared with that of TRAMP$^+$/WT mice showed enrichment in gene sets corresponding to "adipogenesis," "oxidative phosphorylation," and "fatty acid (FA) metabolism," among the three top enriched signatures (Figure 3A). Further analysis using gene ontology (GO) biological process compilation C5 (MSigDb C5) demonstrated that both FA anabolic and catabolic processes were repressed in TRAMP$^+$/p62^{Adipo} mice (Figure 3A). These results indicate that PCa tumors blunt energy-consuming activities such as adipogenesis and mitochondrial oxidative phosphorylation in the p62^{Adipo} WAT. This effect of the tumor shutting down adipose tissue metabolism in the absence of p62 should serve to save nutrients and energy that would be available for the benefit of the tumor to support its own growth. In agreement with this concept, a broad spectrum of genes involved in FA and glycerolipid synthesis for lipogenesis, and their respective upstream regulators, were profoundly repressed in TRAMP$^+$/p62^{Adipo} WAT (Figure 3B). qRT-PCR analysis of inguinal WAT (iWAT) and eWAT confirmed the significant inhibition of key adipogenic (Figures 3C and S3A) and mitochondrial genes (Figures 3D and S3B) under these conditions. Interestingly, these changes in adipose tissue between WT and p62^{Adipo} mice were not observed in the absence of TRAMP tumors (Figures 3C, 3D, S3A, and S3B).

Previous reports have shown that tumors promote energy expenditure in fat by inducing "adipocyte browning" (Kir and Spiegelman, 2016; Petruzzelli et al., 2014). As expected, *Ucp1* levels, a hallmark of that process, was dramatically upregulated, along with other mitochondrial genes, in TRAMP$^+$/WT adipose tissues compared with TRAMP$^-$ controls (Figures 3D and S3B). More importantly, the expression of these genes was not upregulated in p62-deficient adipose tissues (Figures 3D and S3B). To test whether these transcriptional changes affect mitochondrial respiration, we measured oxygen consumption rate (OCR) in WAT explants from the four genotypes. Consistently, respiration was upregulated by PCa tumors in TRAMP$^+$/WT but not in TRAMP$^+$/p62^{Adipo} mice (Figure 3E). Interestingly, the role

of p62 in the control of mitochondrial respiration was also observed in differentiated p62 KO adipocytes when compared with WT controls (Figure 3F). These results demonstrate that the induction of adipose tissue browning by PCa requires p62. Therefore, p62 deficiency in adipocytes prevents the induction of adipose tissue energy utilization and wasting by the TRAMP tumors.

Of mechanistic relevance, further interrogation of the WAT transcriptome revealed that a signature corresponding to mTORC1 signaling was negatively correlated in the WAT of TRAMP$^+$/p62^{Adipo} mice, compared with that of TRAMP$^+$/WT (Figure 3G). Likewise, a "WAT Rapamycin DN" signature was negatively correlated, whereas a "WAT Rapamycin UP" signature was enriched, in TRAMP$^+$/p62^{Adipo} WAT as compared with TRAMP$^+$/WT WAT (Figure S3C). These WAT signatures were obtained from mice treated with rapamycin, a well-established inhibitor of mammalian target of rapamycin complex 1 (mTORC1). These results further support the positive correlation between p62 expression and mTORC1 activation in WAT. Of human relevance, GSEA showed that the transcriptional level of *SQSTM1* positively correlated with mTORC1 signaling enrichment in human WAT (Figures 3H and S3D). The p62 regulation of mTORC1 was confirmed by immunoblotting, which showed a dramatic inhibition of S6 and 4EBP1 phosphorylation, two bona fide downstream targets of mTORC1 (Figure 3I). These are important observations because mTORC1 is a well-recognized regulator of lipogenesis via SREBP1 (Li et al., 2010). Indeed, immunoblotting analysis of the same extracts confirmed reduced levels of FASN in p62-deficient adipose tissue (Figure 3I). Together, these results demonstrate that the reduced activity of mTORC1 in the adipose tissue of p62^{Adipo} mice serves to prevent the activation of energy-consuming pathways in the adipose tissue of PCa-bearing mice, which results in saving nutrients for the benefit of the tumor.

p62 Deficiency in Adipose Tissue Activates Nutrient-Utilizing Pathways in Prostate Tumors

To unravel the mechanisms whereby p62-deficient adipose tissue promotes PCa progression, we carried out a genome-wide transcriptomic analysis of PCa tumors from TRAMP$^+$/WT and TRAMP$^+$/p62^{Adipo} mice. In marked contrast to the general repression of metabolism in the adipose tissue of TRAMP$^+$/p62^{Adipo} mice, GSEA of transcripts upregulated in TRAMP$^+$/p62^{Adipo} tumors revealed a marked enrichment of gene sets associated with FA metabolism, FA β-oxidation, and peroxisome proliferator-activated receptor α (PPARα) activation (Figure 4A and Table S1). There was also a robust increase in FA oxidation genes (Figures 4B and 4C) and, of special relevance, we found increased *Cpt1a* transcript levels, which was confirmed by immunoblotting analysis (Figure 4D). Changes in *Cpt1a* are particularly interesting given the recent description of a critical role of FA oxidation in several types of cancers including PCa (Schlaepfer et al., 2014). Our finding of inverse effects in adipose tissue and PCa tumors in terms of metabolic and energy

(H) GSEA plot of "mTORC1_SIGNALING" signature positively correlated to *SQSTM1* transcript levels in human normal WAT (n = 26, GEO: GSE25402) using H MSigDB collection.
(I) Immunoblots and quantification of mTORC1 downstream targets in ppWAT of TRAMP$^+$/p62^{Adipo} and TRAMP$^+$/WT mice (n = 4).
Results are presented as mean ± SEM (C–F and I). Student's t test (*p < 0.05, **p < 0.01, ***p < 0.001, ****p < 0.0001). See also Figure S3.
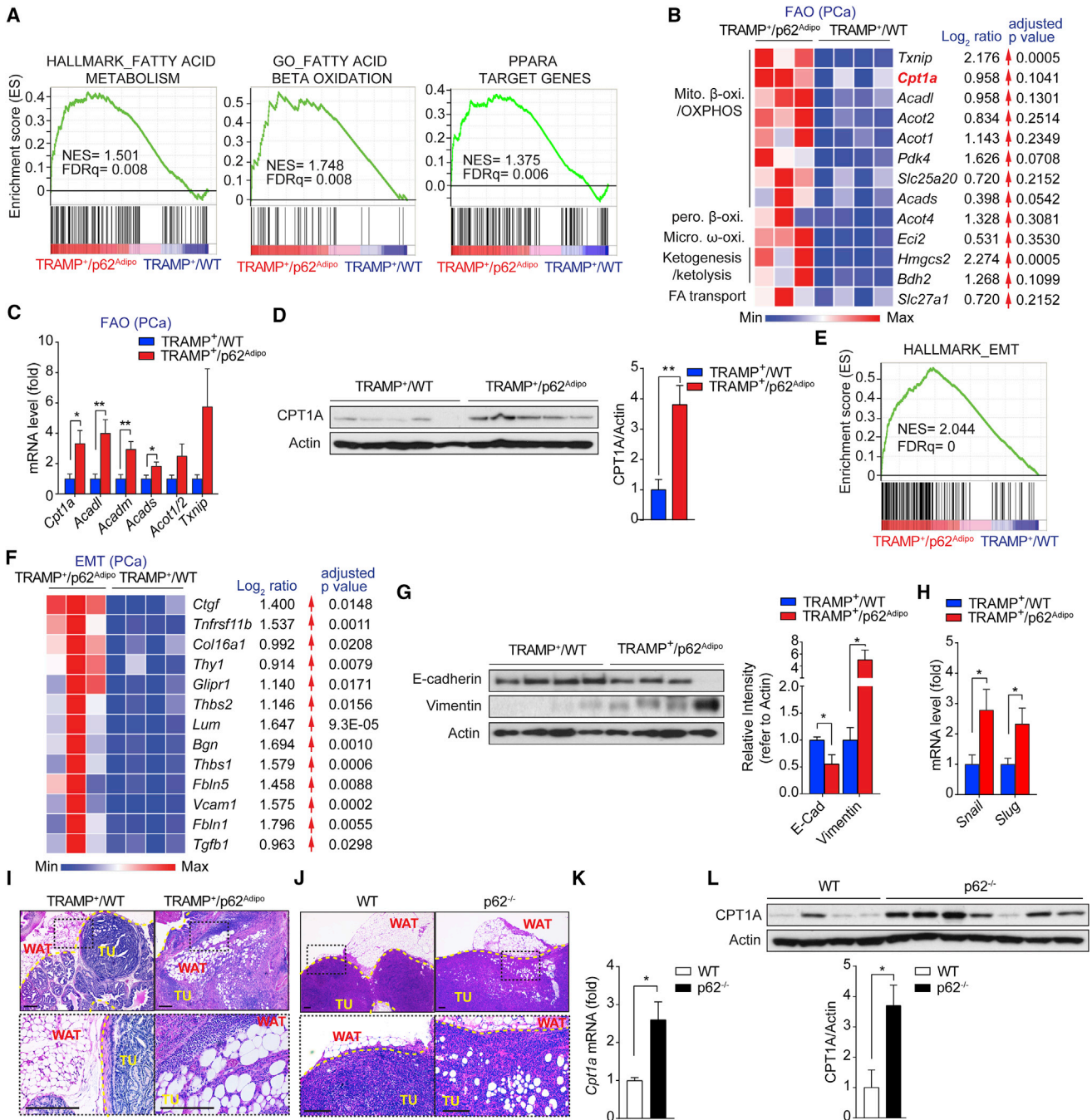
Figure 4. Metabolic Analysis of PCa in TRAMP+/WT and TRAMP+/p62Adipo Mice

(A) GSEA plots of enrichment in GSEA "Hallmark_FA metabolism" (left), "GO_FA β-oxidation" (middle), and "PPARα target gene" (right) signatures in PCa tumors from TRAMP+/p62Adipo (n = 3) versus TRAMP+/WT mice (n = 4).

(B) Leading-edge genes of FA oxidation signature described in right panel of (A).

(C) qPCR analysis of PPARα target genes related to mitochondrial FA oxidation in PCa tumors of TRAMP+/p62Adipo and TRAMP+/WT mice (n = 9).

(D) Immunoblot analysis and quantification of CPT1A in PCa tumors of TRAMP+/p62Adipo versus TRAMP+/WT mice (n = 5, per genotype).

(E) GSEA plot of enrichment in "Hallmark_Epithelial-Mesenchymal-Transition (EMT)" signature in TRAMP+/p62Adipo (n = 3) and TRAMP+/WT mice (n = 4).

(F) Leading-edge genes of EMT signature described in (E).

(G) Immunoblot analysis and quantification of EMT markers in PCa tumors of TRAMP+/p62Adipo versus TRAMP+/WT mice (n = 4, per genotype).

(H) qPCR analysis of EMT drivers (Snail, Slug) in PCa tumors of TRAMP+/p62Adipo and TRAMP+/WT mice (n = 8–9).

utilization triggered by adipocyte-specific deficiency of p62 would explain why the TRAMP tumors can metabolically afford higher degrees of tumorigenesis in p62^Adipo mice in comparison to WT mice. Interestingly, this metabolic rewiring is accompanied by the induction of an epithelial-mesenchymal transition (EMT) signature (Figures 4E and 4F), which is consistent with the increased incidence of metastasis in TRAMP^+/p62^Adipo WAT (Figures 1E–1H). The enriched EMT signature was further supported by immunoblotting, which revealed an inverse correlation of E-cadherin (epithelial) and vimentin (mesenchymal) protein levels in PCa tumors (Figure 4G). Moreover, the EMT transcriptional drivers (*Snail*, *Slug*) were found to be upregulated in TRAMP^+/p62^Adipo tumors (Figure 4H). Histological analysis of TRAMP tumors demonstrated increased invasion in the surrounding adipose tissue as well adipocytes trapped inside the tumor (Figure 4I). Similar results were obtained when orthotopic tumors were analyzed in mice of both genotypes (Figure 4J). This latter system consists in the orthotopic growth of syngeneic PCa cells into the prostate of either WT or p62 KO mice, as described recently (Valencia et al., 2014). Interestingly, and in keeping with the upregulation of *Cpt1a* in the tumors of TRAMP^+/p62^Adipo mice, TRAMP orthotopic tumors grown in p62 KO mice also displayed higher levels of *Cpt1a* transcripts and protein levels (Figures 4K and 4L). Collectively these results demonstrate that the loss of p62 in the adipose tissue increases PCa cancer aggressiveness and metastasis, which correlates with enhanced invasion and the upregulation of *Cpt1a*.

Role of Adipocyte-Specific p62 Deficiency in Tumor Growth and Invasion

To study in more detail the mechanisms whereby adipocyte's p62 controls the metabolic and cellular crosstalk between PCa tumors and the adipose tissue *in vivo*, we carried out a series of *in vitro* studies using organotypic cultures. This is a 3D *in vitro* system that recapitulates the tumor microenvironment (Valencia et al., 2014). We have successfully set up 3D cultures with adipocytes that maintain the unilocular structure and active functions of adipocytes *in vitro* (Figure 5A). We initially cultured minced adipose tissue from WT or p62 KO mice embedded in the collagen I/Matrigel matrix combined with PCa cells seeded on top of the gel, and evaluated the impact of p62-deficient adipose tissue explants on prostate cell invasion. The ability of p62-deficient WAT to promote PCa invasion was significantly larger than that of WT WAT (Figures 5B and 5C). We then separated mature adipocytes and stromal vascular fraction (SVF) containing preadipocytes, endothelial cells, macrophages, and adipocyte stem cells, and tested them in organotypic cultures. Interestingly, mature adipocytes, as well as the whole SVF from p62 KO mice, produced a marked increase in PCa invasion (Figures 5D–5G), whereas macrophages had no effect (Valencia et al., 2014). Two-chamber co-culture studies, as described in Figure 5H, showed that exposure of TRAMP-C2RE3 and Myc-CAP cells to conditioned medium (CM) from p62 KO WAT pro-

moted higher levels of migration (Figures 5I, 5J, and S4A) and invasion (Figures 5K, 5L, and S4B), respectively. Together these results demonstrate that adipocyte's p62 plays a critical role in the control of the secretion of molecules that are central in the regulation of the ability of PCa cells to migrate and invade, which underlies the more invasive and metastatic phenotype of TRAMP^+/p62^Adipo mice.

Loss of p62 in Adipose Tissue Results in Enhanced Osteopontin Synthesis

A critical question is the identification of the factor(s) secreted by the p62-deficient adipose tissue. Since increased adiposity is associated with enhanced inflammation, which might be important for tumor progression (De Marzo et al., 2007; Ouchi et al., 2011), we characterized the inflammatory response both in adipose tissue and in PCa tumors from TRAMP^+/WT and TRAMP^+/p62^Adipo mice. Of note, the adipose tissue from non-tumor-bearing p62^Adipo mice showed a significant increase in crown-like structure (CLS) compared with WT mice (Figures 6A and 6B), consistent with the enhanced inflammation previously reported in the adipose tissue of these mutant mice (Muller et al., 2013; Rodriguez et al., 2006). However, this inflammatory response was dramatically intensified in the adipose tissue of tumor-bearing TRAMP^+/p62^Adipo mice (Figures 6A and 6B). Therefore, the combination of p62 deficiency in adipocytes, along with the presence of prostate tumors, results in a considerably increased inflammatory response in the adipose tissue. To further analyze this effect, we applied CIBERSORT to our RNA-sequencing data, which revealed a significant decrease in the infiltration of M1 macrophages in TRAMP^+/p62^Adipo adipose tissue as compared with TRAMP^+/WT controls (Figure 6C). Further analysis showed higher expression of M2 markers such as *Arg1* and *Mgl2* (Figure 6D), indicating an enrichment toward the M2 lineage. Importantly, there was a dramatic upregulation in the levels of *Spp1* (coding osteopontin [OPN]) (Figure 6D). This is of particular relevance, since high levels of OPN expression in M2-polarized macrophages are essential for the remodeling of the adipogenic cell niche (Lee et al., 2013) and for tumorigenesis (Ahmed et al., 2016). Therefore, we next compared the adipose tissue secretomes of TRAMP^+/p62^Adipo and TRAMP^+/WT mice. Interestingly, the most highly expressed transcript corresponding to a secreted protein was *Spp1* (Figures 6E and S5A). Consistent with this, serum levels of OPN were increased in TRAMP^+/p62^Adipo mice compared with WT controls (Figure 6F). Notably, OPN expression was also upregulated in the adipose tissue of tumor-free p62^Adipo mice (Figures 6G and 6H). This indicates that p62 deficiency in the adipose tissue results in OPN expression that is further amplified by the TRAMP tumor. The similarity in the expression pattern of OPN (Figure 6H) and F4/80 (Figure 6A) suggests a strong association between OPN overexpression and macrophage infiltration in WAT. Interestingly, immunofluorescence analysis of the adipose tissue revealed that OPN was not only

---

(I and J) H&E staining of periprostatic WAT adjunct to PCa tumor from TRAMP^+/p62^Adipo and TRAMP^+/WT controls (I) and of orthotopic tumors from p62 KO mice and WT mice (J). WAT: white adipose tissue; TU: prostate tumor. Scale bars, 200 μm.

(K) qPCR analysis of *Cpt1a* mRNA expression in orthotopic prostate tumors of p62 KO (n = 7) and WT mice (n = 4).

(L) Immunoblot analysis and quantification of CPT1A expression in orthotopic tumors described in (K).

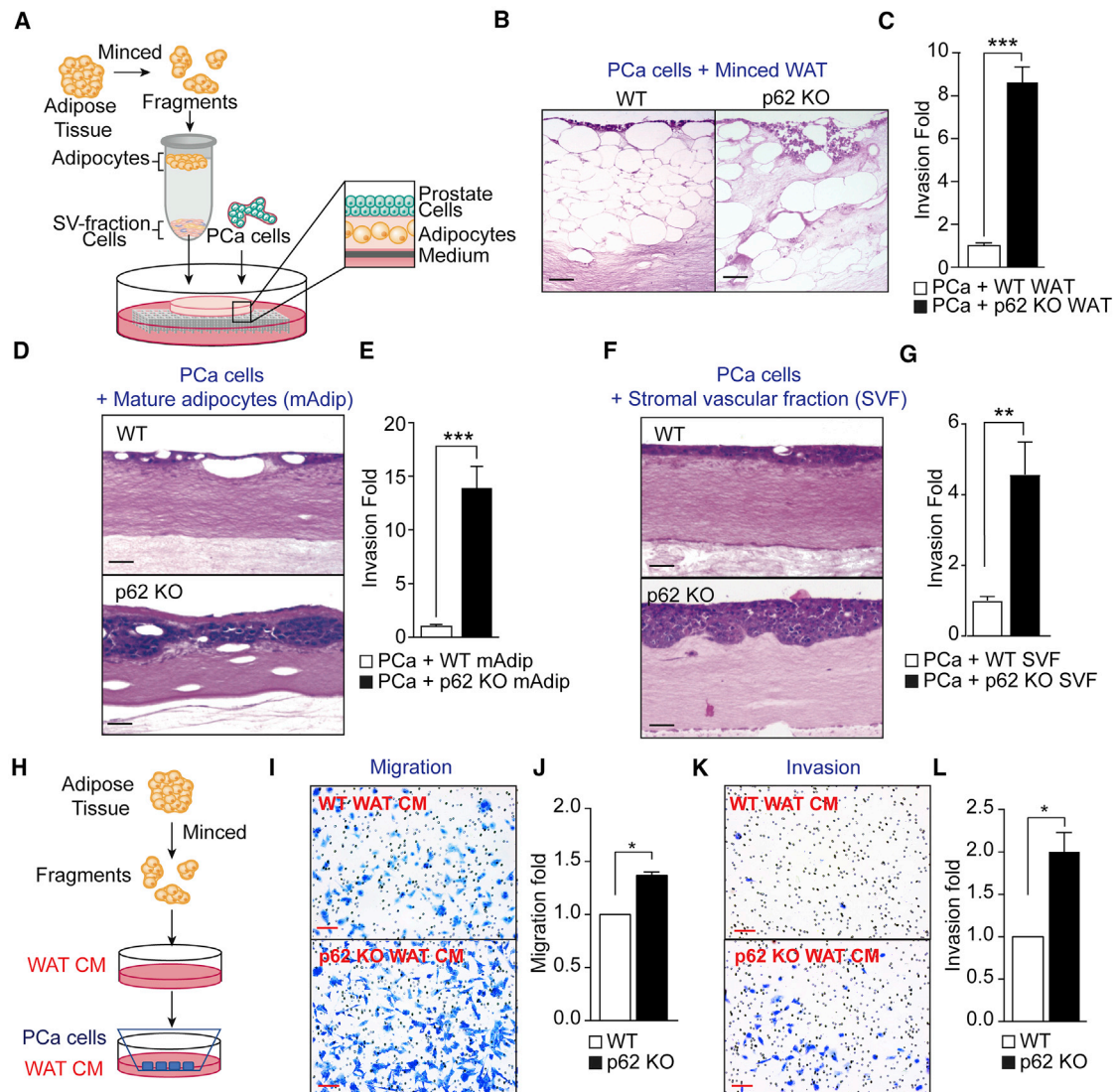Results are presented as mean ± SEM (C, D, G, H, K, L). Student's t test (*p < 0.05, **p < 0.01). See also Table S1.

Figure 5. Role of p62 in the Adipose Tissue-PCa Cell Interaction *In Vitro*

(A) Schematic representation of 3D organotypic cultures used to study the interaction between adipose tissue and PCa cells.

(B and C) H&E staining of organotypic gels of Myc-Cap cells cultured in the presence of minced WAT from WT or p62 KO mice (B) and quantification of PCa cell invasion (C) (n = 8). Scale bars, 100 μm.

(D–G) H&E staining of organotypic gels of Myc-Cap cells cultured in the presence of mature adipocytes (n = 5–8) (D) or SVF (n = 9) (F) from the indicated genotypes and quantification of PCa cell invasion of these cultures (E and G). Scale bars, 100 μm.

(H) Schematic illustration of tumor migration and invasion assays as determined in Transwell system using WAT conditioned medium (CM) as chemoattractant.

(I and J) Migration of TRAMP-C2RE3 cells in response to CM of p62 KO WAT or WT control for 16 hr. Representative images (I) and quantification (J) of three independent experiments (n = 3). Scale bars, 100 μm.

(K and L) Invasion of TRAMP-C2RE3 cells in response to CM as described in (I) for 22 hr. Representative images (K) and quantification (L) of three independent experiments (n = 3). Scale bars, 100 μm.

Results are presented as mean ± SEM (C, E, G, J, L). Student's t test (*p < 0.05, **p < 0.01, ***p < 0.001). See also Figure S4.

expressed in the CLS niche (identified by F4/80) in p62^Adipo WAT, but also in adipocytes that were not located in CLS, whereas OPN was almost undetectable in WT WAT (Figure 6I). *Spp1* mRNA levels were also increased in primary adipocytes but not in macrophages both isolated from eWAT of p62^Adipo mice (Figure S5B). Furthermore, OPN protein levels were also increased in SVF-differentiated p62 KO adipocytes (Figure S5C), suggesting that OPN derived from adipocytes is the primary

driver of the phenotype. Analysis of tumors from TRAMP^+/p62^Adipo mice showed enhanced expression of *Spp1* transcripts (Figure 6J). Furthermore, GSEA of the TRAMP^+/p62^Adipo PCa transcriptome revealed an enrichment in the PRAD_SPP1 signature compared with TRAMP^+/WT tumors (Figure 6K). This signature was created with the top *SPP1* most correlated genes from the TCGA_PRAD dataset, further demonstrating the human relevance of the increased OPN levels in the
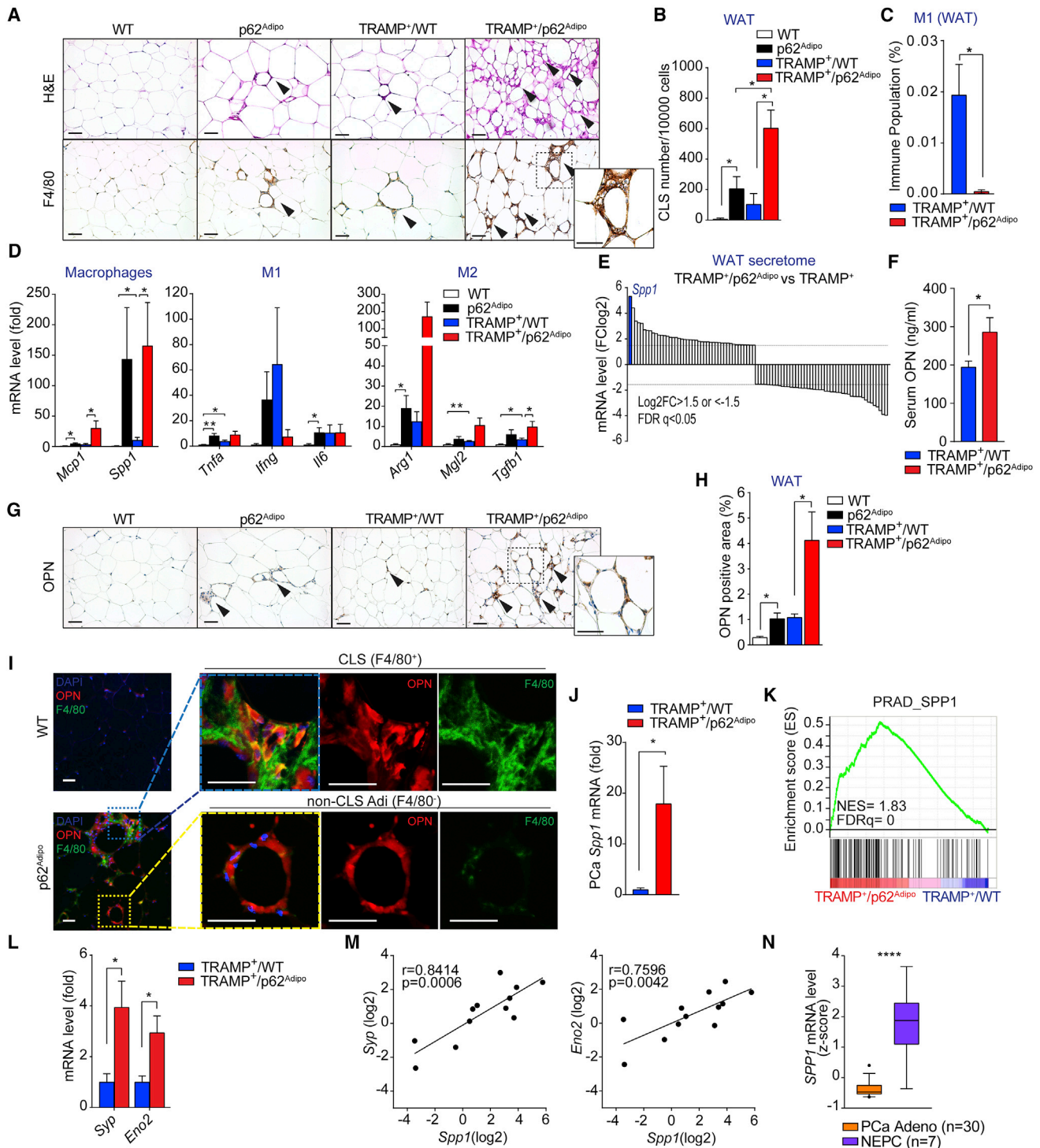
Figure 6. Loss of p62 in Adipose Tissue Results in Enhanced OPN Synthesis

(A) H&E staining (top) and F4/80 IHC (bottom) in eWAT. Black arrowheads indicate CLS (n = 3–4, per genotype). Scale bars, 100 μm.

(B) Quantification of CLS number in eWAT (n = 4, per genotype).

(C) Estimated abundance of "M1" macrophage population in eWAT (n = 3) by CIBERSORT analysis.

(D) qPCR analysis of inflammation markers in eWAT (n = 5–6, per genotype).

(E) Secretome analysis in eWAT. The predicted 90 candidates were sorted by fold change of expression in TRAMP⁺/p62^Adipo versus TRAMP⁺/WT WAT (n = 3, per genotype).

(F) Determination of serum OPN concentrations in TRAMP⁺/p62^Adipo and TRAMP⁺/WT mice (n = 7, per genotype).

(legend continued on next page)

TRAMP$^+$/p62^{Adipo} tumors. Consistent with the observed increased frequency of neuroendocrine differentiation, PCa tumors from TRAMP$^+$/p62^{Adipo} mice have higher levels of *Synaptophysin* (*Syp*) and *Enolase 2* (*Eno2*), two well-established neuroendocrine markers (Figure 6L). Of note, *Spp1* mRNA levels positively correlated with the expression of *Syp* and *Eno2* in TRAMP tumors (Figure 6M). Consistent with this result, and of human relevance, the levels of OPN were also increased when neuroendocrine tumors were compared with adenocarcinoma in human PCa samples (Figure 6N) (Beltran et al., 2011). Altogether these results support a role for OPN in mediating tumor aggressiveness driven by adipocyte p62 deficiency.

Osteopontin Promotes Tumor Invasion and Migration through CPT1A

Since p62 deficiency in adipocytes promotes the upregulation of CPT1A in TRAMP tumors, we next determined its potential role in PCa cell migration, invasion, and proliferation. To this end, we generated Myc-CAP and TRAMP-C2RE3 PCa cells deficient in CPT1A by using short hairpin RNA (shRNA) vectors. Boyden chamber Transwell studies demonstrated that CPT1A deficiency diminished the invasive capacity of two different types of PCa cells (Figures 7A and S6A). Moreover, PCa cell proliferation was also hampered by CPT1A deficiency (Figure S6B). Organotypic studies co-culturing minced adipose tissue from WT or p62^{Adipo} mice with CPT1A-proficient or -deficient Myc-CAP PCa cells demonstrated that the ability of p62^{Adipo} WAT to promote the invasion of Myc-Cap cells was severely inhibited by CPT1A deficiency (Figure 7B). Interestingly, PCa cell invasion stimulated by CM from p62-deficient but not from WT WAT was also abrogated by CPT1A inactivation either by shRNA (Figure 7C) or the addition of the CPT1 chemical inhibitor, etomoxir (Figure 7D). Since the adipocyte-specific deletion of p62 results in upregulated *Spp1* also in PCa tumors (Figure 6K), we next determined whether OPN is sufficient to promote PCa cell migration and invasion and whether that requires CPT1. Interestingly, exposure of Myc-CAP and TRAMP-C2RE3 cells to OPN was sufficient to promote their migration and invasion, which were totally abrogated by CPT1A deficiency (Figures 7E, 7F, S6C, and S6D). We also found that incubation of Myc-CAP PCa cells with OPN was sufficient to drive cell proliferation, which was abolished by CPT1A deficiency (Figure S6E). We next determined whether OPN could upregulate CPT1 expression, and whether this resulted in increased FA oxidation (FAO) in PCa cells. Notably, CPT1A protein levels in Myc-CAP cells were significantly elevated upon OPN treatment (Figure 7G). Importantly, *in vitro* culture of TRAMP$^+$ prostate organoids with OPN resulted in enhanced OCR (Figure 7H). This effect was abrogated

by treatment with etomoxir, demonstrating the contribution of FAO to the OPN-enhanced OCR (Figure 7H). Of note, the transcript levels of *Cpt1a*, and its upstream regulator *Ppara*, were upregulated by OPN in organoids (Figure 7I).

Importantly, bioinformatics analysis in different human PCa datasets showed that the levels of *SPP1* transcripts and those of two CPT1 isoforms (*CPT1A*, *CPT1B*), as well as of another FAO gene, *ACAD9*, were concomitantly elevated in prostate cancer, showing the highest levels in metastases (Figures 7J, S6F, and S6G). Further data mining revealed significant positive correlations of *SPP1* with *CPT1B* and *ACAD9* transcripts in several human PCa datasets, including a cohort of human castration-resistant PCa patients (Beltran et al., 2016) (Figures 7K, S6H, and S6I). Interrogation of a large TCGA cohort of prostate adenocarcinoma patients demonstrated the significant positive correlation between Gleason score and the expression of *SPP1*, *CPT1A*, and *ACAD9* (Figures 7L and S6J). We next analyzed the biochemical recurrence in these patients, which were categorized into four groups based on the co-expression of *SPP1* and two *CPT1* isoforms, as well as of *ACAD9*. Of clinical significance, the prognostic outcome was the worst in patients with the highest expression of both *SPP1* together with either *CPT1* or *ACAD9* (Figures 7M and S6K). Collectively, these results demonstrate that p62 deficiency in the adipose tissue systemically upregulates the expression of OPN, which is critical for PCa proliferation, migration, and invasion, through a Cpt1a-dependent mechanism.

DISCUSSION

Epidemiological data and studies in mice are progressively establishing the importance of obesity in cancer. Although the contribution of exacerbated food intake to the metabolic syndrome and its role in cancer incidence and progression is evident, the molecular underpinnings of how whole metabolism and obesity affect tumorigenesis still need to be fully understood. A common confounding factor in this type of research is that most of these studies involve feeding mice with high-fat diets. Here we profited from a previous mouse model system developed in our laboratory in which the selective genetic inactivation of p62 in the adipose tissue results in increased adiposity and obesity in a manner that is independent of food intake or locomotor activity (Muller et al., 2013). In this system, we can interrogate how the adipose tissue modulates tumorigenesis and how tumors affect fat tissues, independently of dietary conditions. Using our model, we found that the specific genetic inactivation of p62 in adipocytes promotes a more aggressive phenotype in tumor-bearing mice. Furthermore, we demonstrate

---

(G and H) OPN IHC staining (G) and quantification of percentage of OPN-positive staining area (H) in eWAT (n = 3–5, per genotype). Black arrowheads indicate OPN staining. Scale bars, 100 μm.

(I) OPN and F4/80 double immunofluorescence staining in eWAT of p62^{Adipo} and WT mice (n = 3, per genotype). CLS niche (F4/80 positive) and non-CLS adipocytes (F4/80 negative) were selected and highlighted in dashed boxes. Scale bars, 100 μm.

(J) qPCR analysis of *Spp1* mRNA expression in PCa tumors of TRAMP$^+$/p62^{Adipo} and TRAMP$^+$/WT mice (n = 6, per genotypes).

(K) GSEA plot of enrichment in "TCGA_SPP1" signature in PCa tumors of TRAMP$^+$/p62^{Adipo} (n = 3) versus TRAMP$^+$/WT mice (n = 4).

(L) qPCR analysis of NE markers in PCa tumors of TRAMP$^+$/p62^{Adipo} and TRAMP$^+$/WT mice (n = 6, per genotypes).

(M) Scatterplots of expression of *Spp1* related to *Syp* (left) or *Eno2* (right) in TRAMP$^+$ tumors (n = 12). Pearson's correlation analysis.

(N) Box-and-whisker plots of *SPP1* transcripts in human patient samples of either NE prostate cancer (NEPC) or adenocarcinoma (Adeno). Data were extracted from dataset (Beltran et al., 2011). Mann-Whitney test.

Results are presented as mean ± SEM (B–D, F, H, J, L). Student's t test (*p < 0.05, **p < 0.01, ****p < 0.0001). See also Figure S5.
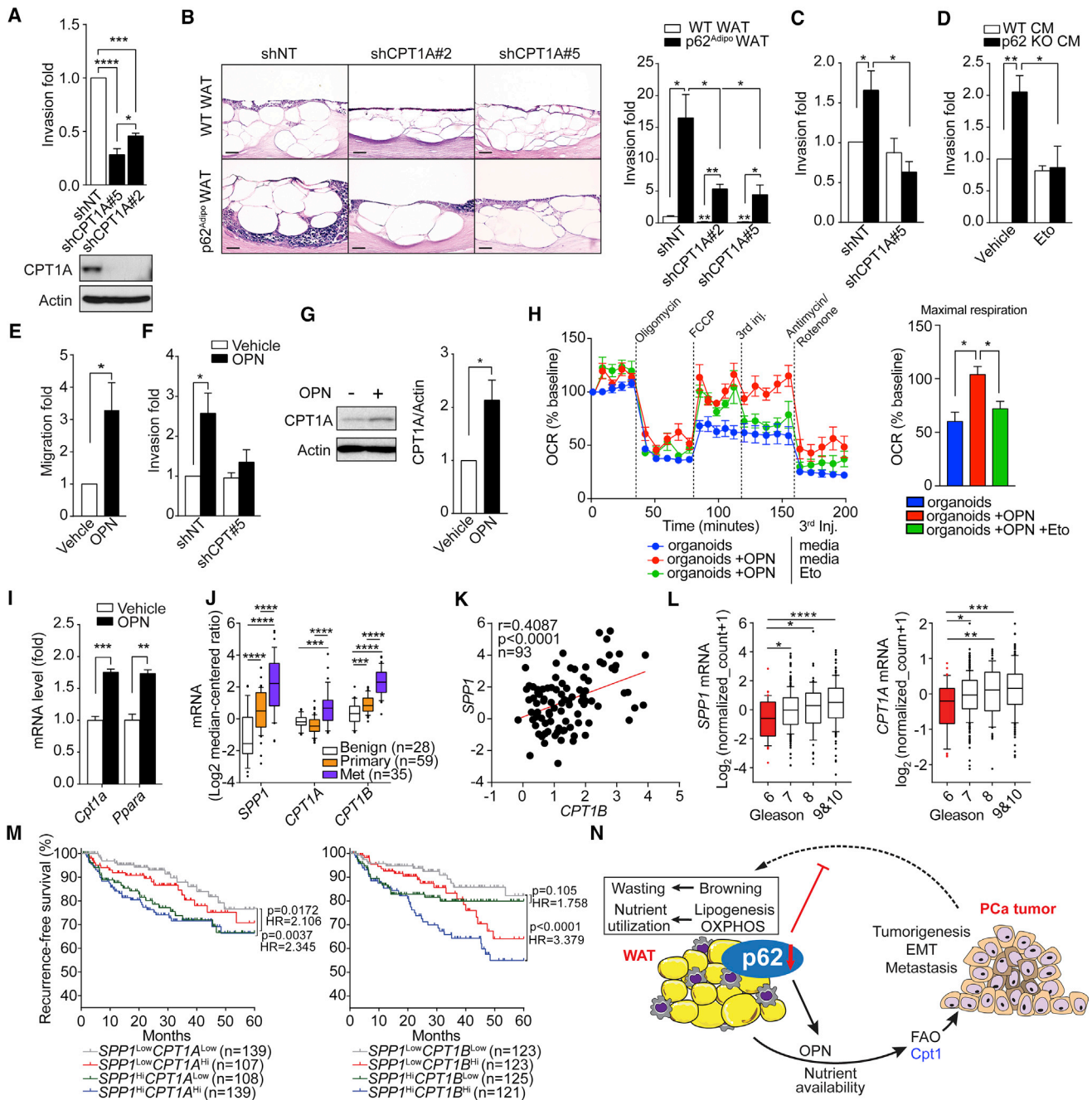
Figure 7. Cpt1a Is Required for OPN-Stimulated Proliferation and Invasion in PCa Tumor

(A) Cell invasion of Myc-CAP (right) deficient in *Cpt1a* (shCPT1A) or control (shNT) in response to 5% fetal bovine serum (FBS) DMEM in Transwell system for 20 hr. Three independent experiments (n = 3). Bottom: immunoblot of CPT1A in cells.

(B) H&E staining and quantification of cell invasion of organotypic gels culturing Myc-Cap cells described in (A) in the presence of minced WAT from WT or p62^{Adipo} mice. Three independent experiments (n = 3). Scale bars, 100 μm.

(C and D) Cell invasion of TRAMP-C2RE3 in response to conditioned medium (CM) of p62 KO WAT or WT controls in Transwell system for 22 hr (n = 4). TRAMP-C2RE3 were either deficient in *Cpt1a* (shCPT1A) (C) or treated with 100 μM etomoxir (Eto) (D). In the etomoxir group, cells were pretreated with etomoxir 8 hr prior to CM stimulation.

(E) Cell migration of Myc-CAP in response to recombinant OPN (5 μg/mL) in Transwell system for 20 hr (n = 5).

(F) Cell invasion of Myc-Cap (shCPT1A or shNT) in response to recombinant OPN (5 μg/mL) in Transwell system for 24 hr, respectively (n = 4).

(G) Immunoblot analysis and quantification of CPT1A in Myc-CAP treated with OPN (3 μg/mL) in medium containing 2% FBS for 24 hr (n = 5).

(H) Seahorse OCR measurement in prostate organoids isolated from 2-month-old TRAMP$^+$/WT mice (n = 3). Organoids were treated with OPN (3 μg/mL) for 5 days before measurement. In the Eto group, etomoxir was injected at port C to block FA oxidation. Right: quantification of maximal respiration rate.

(I) qPCR analysis of *Cpt1a* and *Ppara* mRNA expression in OPN-treated organoids as described in (H) (n = 3).

that this correlates with the activation of gene expression networks in the tumor consistent with EMT, which explains the more metastatic and invasive behavior of tumors in TRAMP[+]/p62[Adipo] mice.

Notably, the more aggressive phenotype of tumors from TRAMP[+]/p62[Adipo] mice correlated with the enhanced expression of a series of metabolic genes consistent with a higher lipid metabolism and increased FAO, including *Cpt1a*. This is very important because FAO is considered the dominant bioenergetics pathway in non-glycolytic tumors such as PCa (Liu, 2006). This metabolic reprogramming orchestrated by the loss of p62 in adipocytes would serve to help the tumor cope with the high energy demand of a more aggressive cancer. Previous reports showed that FAs were provided by proximal adipose tissue for the growth of ovarian cancer cells (Nieman et al., 2011). This adipocyte-tumor connection is complemented by a reverse link whereby tumors also affect the metabolic state of adipocytes. In this regard, the loss of adipocyte's p62 also favors tumorigenesis by preventing the activation by the tumor of the expression of genes critical for FA anabolism in the adipose tissue. Therefore, we unveil a p62-repressed mechanism for the adipose tissue to contribute to tumor growth by reducing the accumulation of energy in the fat reservoir, making it available for its utilization by the tumor in the form of FAs that will be burned by cancer cells. Furthermore, we also demonstrate that p62 in adipocytes is required for the ability of PCa to upregulate gene expression networks of mitochondrial biogenesis in the adipose tissue. In this way, tumor actions that result in enhanced nutrient utilization and energy wasting in the adipose tissue were abolished in the absence of p62, favoring the utilization of energy by the tumor. Many studies demonstrated that mTORC1 signaling is central to the maintenance of white adipose tissue function due to its essential role in adipogenesis (Cai et al., 2016). Interestingly, and in agreement with our previously reported data demonstrating a critical role of p62 in mTORC1 activation by nutrients (Duran et al., 2011; Linares et al., 2015), we show here that the p62-deficient adipose tissue displayed reduced mTORC1 activity. Therefore, p62's role in the metabolism of a tumor-bearing organism is to maintain the activity of adipocyte's mTORC1. This is very important because fat is the key reservoir of body energy. Therefore, although the tumor promotes the metabolic activation of the adipose tissue, which paradoxically would result in fewer nutrients available for its own growth, p62 deficiency (likely by reducing mTORC1 activity in adipocytes) favors the organism response to reduce energy utilization in the fat, favoring the access of PCa tumors to FA to fulfill the tumor's energetic needs through the upregulation of

CPT1 and the subsequent increase in FAO. Based on these observations, we can predict that a potential side effect of mTORC1 inhibitors in cancer therapy will be the potentiation of the tumor effects on the metabolic shutdown of the adipose tissue, which undoubtedly will favor tumor metabolism and growth.

Our results must also be put in the context of what is already known regarding the communication between tumor and the adipose tissue. It is very well established that certain cancers promote the activation of a metabolic program driven by the "browning" of WAT (Kir and Spiegelman, 2016; Petruzzelli et al., 2014). This phenomenon of fat cachexia results in enhanced fat energy burning, which leads to tissue wasting, similarly to what takes place during muscle cachexia. In the case of fat cachexia, the gain for the tumor is not totally apparent since uncoupled mitochondrial activation in adipocytes by the tumor results in wasting of energy that the tumor desperately needs to proliferate. Our data are of great relevance because we demonstrate that the loss of p62 in adipocytes severely inhibits WAT browning by the tumor, unveiling the existence of a previously unappreciated and completely different mechanism of p62-controlled fat-tumor communication. Thus, instead of activating adipose energy expenditure as occurs during browning cachexia, the tumor and the adipose tissue establish a symbiotic interaction whereby the low energy utilization of the adipose tissue in the absence of p62 helps the high energetic demands of the tumor. These data are consistent with the general concept that has emerged recently whereby although p62 might function as a tumor promoter in the cancer epithelium, it plays a non-cell-autonomous role as tumor suppressor in the microenvironment (Moscat et al., 2016; Reina-Campos et al., 2017).

Another critical question arising from the studies reported here is the nature of the signal generated by the loss of p62 in adipocytes that makes PCa tumors more aggressive and more metabolically active through the upregulation of Cpt1a and FAO. Our results demonstrate that OPN plays a central role in this process, which is consistent with other studies suggesting the implication of this multifunctional molecule in inflammation, cell migration, and tissue remodeling, contributing to a variety of cancers including PCa (Rangaswami et al., 2006). Thus, elevated OPN levels in patients' tumor tissue and blood were correlated with metastatic potential and poor prognosis (Shevde et al., 2010). OPN can be expressed by both tumor cells and cellular components of the tumor microenvironment, such as macrophages (Ahmed et al., 2016; Lee et al., 2013). In this regard, our data integrate previously reported roles for OPN in cancer by unveiling a molecular link between adipose tissue and tumor epithelium through the control of cancer metabolism in a

(J) Box-and-whisker plots of *CPT1A* and *1B* transcript levels in prostate samples from different lesion sites in human prostate cancer dataset (Grossa 2012) extracted from Oncomine. Median (horizontal line), interquartile range (box), and 10th–90th percentiles (whiskers). Mann-Whitney test.

(K) Scatterplots of expression of *SPP1* related to *CPT1B* in patient samples (n = 93) from dataset described in (J). Pearson's correlation analysis.

(L) Box-and-whisker plots of *SPP1* (left) and *CPT1A* (right) transcript levels in patients with different Gleason Scores from TCGA PRAD dataset. Gleason 6 (n = 45), 7 (n = 247), 8 (n = 64), 9 plus 10 (n = 142). Mann-Whitney test.

(M) Kaplan-Meier curve of 5-year freedom from biochemical recurrence in patients from TCGA PRAD cohort (n = 493) according to *SPP1* and *CPT1A* (left) or *SPP1* and *CPT1B* (right) co-expression. Median as expression cutoff. Log-rank test. HR, hazard ratio.

(N) Schematic representation of the proposed role of adipocyte p62 in crosstalk between PCa tumor and adipose tissue. PCa tumors promotes browning, lipogenesis, and OXPHOS in adipose tissue. Loss of p62 in adipocytes results in insufficient browning and energy utilization by adipocytes, preserving more nutrients and secreting OPN for the demand of PCa tumors that could facilitate tumorigenesis and metastasis through FAO.

Results are presented as mean ± SEM except (A) to (I). *p < 0.05, **p < 0.01, ***p < 0.001, ****p < 0.0001. Student's t test unless indicated otherwise. See also Figure S6.

non-cell-autonomous and p62-dependent manner. We establish here that although the expression of OPN is enhanced not only in adipocytes of TRAMP$^+$/p62^{Adipo} mice but also in macrophages and tumors, the initiating event is the selective loss of p62 in adipocytes since the levels of p62 in macrophages and tumors are not reduced. Therefore, an interesting question for future studies is how p62 deficiency in adipocytes triggers the synthesis of OPN. However, irrespective of that mechanism, what is important is that we demonstrate here that OPN is a central link between the pro-tumorigenic adipose tissue and the cancer cell through the upregulation of CPT1 and the generation of the energy required for the tumor to acquire a more invasive and metastatic phenotype. These findings are of clinical relevance since the analysis of the human castration-resistant PCa dataset demonstrates a significant correlation between OPN transcripts and those of Cpt1, which also positively correlated with Gleason score and metastasis in human PCa. In summary, our model (Figure 7N) proposes a systemic communication between PCa tumors and fat, resulting in antithetic metabolic reprogramming in both tissues, which ultimately results in increased tumor malignancy.

STAR★METHODS

Detailed methods are provided in the online version of this paper and include the following:

- KEY RESOURCES TABLE
- CONTACT FOR REAGENT AND RESOURCE SHARING
- EXPERIMENTAL MODEL AND SUBJECT DETAILS
  - Mouse Models
  - Cell Lines
- METHOD DETAILS
  - Indirect Calorimetry
  - Body Composition Measurements
  - Immunoblot Analysis
  - Histological Analysis
  - Lipid Analysis
  - Adipose Tissue Conditioned Media
  - Migration and Invasion Assay
  - RNA Analysis
  - Organotypic Cultures
  - Respiration Assays
  - RNAseq, Gene Set Enrichment Analysis, CIBERSORT and Secretome Analysis
  - Bioinformatic Analysis of Clinical Data
- QUANTIFICATION AND STATISTICAL ANALYSIS
- DATA AND SOFTWARE AVAILABILITY

SUPPLEMENTAL INFORMATION

Supplemental Information includes six figures and two tables and can be found with this article online at https://doi.org/10.1016/j.ccell.2018.03.001.

AUTHOR CONTRIBUTIONS

J.H. performed most of the experiments. A.D. generated mouse lines and contributed to immunofluorescence and Seahorse data. M.R.-C. conducted the organoid experiments and assisted in the bioinformatics analyses. T.V. performed orthotopic injections and contributed to organotypic experiments. E.A.C. and A.D. provided pathological analysis. T.D.M. and M.H.T. provided p62$^{f/f}$aP2-Cre mice and expertise in mouse metabolism. All authors discussed the results and commented on the manuscript. M.T.D.-M. and J.M. conceived and supervised the project. M.T.D.-M. and J.M. wrote the manuscript with help of J.H.

REFERENCES

Ahmed, M., Sottnik, J.L., Dancik, G.M., Sahu, D., Hansel, D.E., Theodorescu, D., and Schwartz, M.A. (2016). An osteopontin/CD44 axis in RhoGDI2-mediated metastasis suppression. Cancer Cell 30, 432–443.

Beltran, H., Prandi, D., Mosquera, J.M., Benelli, M., Puca, L., Cyrta, J., Marotz, C., Giannopoulou, E., Chakravarthi, B.V., Varambally, S., et al. (2016). Divergent clonal evolution of castration-resistant neuroendocrine prostate cancer. Nat. Med. 22, 298–305.

Beltran, H., Rickman, D.S., Park, K., Chae, S.S., Sboner, A., MacDonald, T.Y., Wang, Y., Sheikh, K.L., Terry, S., Tagawa, S.T., et al. (2011). Molecular characterization of neuroendocrine prostate cancer and identification of new drug targets. Cancer Discov. 1, 487–495.

Brawley, O.W. (2012). Trends in prostate cancer in the United States. J. Natl. Cancer Inst. Monogr. 2012, 152–156.

Cai, H., Dong, L.Q., and Liu, F. (2016). Recent advances in adipose mtor signaling and function: therapeutic prospects. Trends Pharmacol. Sci. 37, 303–317.

Calle, E.E., and Kaaks, R. (2004). Overweight, obesity and cancer: epidemiological evidence and proposed mechanisms. Nat. Rev. Cancer 4, 579–591.

Calle, E.E., Rodriguez, C., Walker-Thurmond, K., and Thun, M.J. (2003). Overweight, obesity, and mortality from cancer in a prospectively studied cohort of U.S. adults. N. Engl. J. Med. 348, 1625–1638.

Cao, Y., and Ma, J. (2011). Body mass index, prostate cancer-specific mortality, and biochemical recurrence: a systematic review and meta-analysis. Cancer Prev. Res. (Phila.) 4, 486–501.

De Marzo, A.M., Nakai, Y., and Nelson, W.G. (2007). Inflammation, atrophy, and prostate carcinogenesis. Urol. Oncol. 25, 398–400.

Duran, A., Amanchy, R., Linares, J.F., Joshi, J., Abu-Baker, S., Porollo, A., Hansen, M., Moscat, J., and Diaz-Meco, M.T. (2011). p62 is a key regulator of nutrient sensing in the mTORC1 pathway. Mol. Cell 44, 134–146.

Duran, A., Serrano, M., Leitges, M., Flores, J.M., Picard, S., Brown, J.P., Moscat, J., and Diaz-Meco, M.T. (2004). The atypical PKC-interacting protein p62 is an important mediator of RANK-activated osteoclastogenesis. Dev. Cell 6, 303–309.

Finkelstein, E.A., Ruhm, C.J., and Kosa, K.M. (2005). Economic causes and consequences of obesity. Annu. Rev. Public Health 26, 239–257.

Finley, D.S., Calvert, V.S., Inokuchi, J., Lau, A., Narula, N., Petricoin, E.F., Zaldivar, F., Santos, R., Tyson, D.R., and Ornstein, D.K. (2009). Periprostatic adipose tissue as a modulator of prostate cancer aggressiveness. J. Urol. 182, 1621–1627.

Freedland, S.J., and Platz, E.A. (2007). Obesity and prostate cancer: making sense out of apparently conflicting data. Epidemiol. Rev. *29*, 88–97.

Greenberg, N.M., DeMayo, F., Finegold, M.J., Medina, D., Tilley, W.D., Aspinall, J.O., Cunha, G.R., Donjacour, A.A., Matusik, R.J., and Rosen, J.M. (1995). Prostate cancer in a transgenic mouse. Proc. Natl. Acad. Sci. USA *92*, 3439–3443.

Ittmann, M., Huang, J., Radaelli, E., Martin, P., Signoretti, S., Sullivan, R., Simons, B.W., Ward, J.M., Robinson, B.D., Chu, G.C., et al. (2013). Animal models of human prostate cancer: the consensus report of the New York meeting of the Mouse Models of Human Cancers Consortium Prostate Pathology Committee. Cancer Res. *73*, 2718–2736.

Keto, C.J., Aronson, W.J., Terris, M.K., Presti, J.C., Kane, C.J., Amling, C.L., and Freedland, S.J. (2012). Obesity is associated with castration-resistant disease and metastasis in men treated with androgen deprivation therapy after radical prostatectomy: results from the SEARCH database. BJU Int. *110*, 492–498.

Kir, S., and Spiegelman, B.M. (2016). Cachexia & brown fat: a burning issue in cancer. Trends Cancer *2*, 461–463.

Lee, Y.H., Petkova, A.P., and Granneman, J.G. (2013). Identification of an adipogenic niche for adipose tissue remodeling and restoration. Cell Metab. *18*, 355–367.

Li, S., Brown, M.S., and Goldstein, J.L. (2010). Bifurcation of insulin signaling pathway in rat liver: mTORC1 required for stimulation of lipogenesis, but not inhibition of gluconeogenesis. Proc. Natl. Acad. Sci. USA *107*, 3441–3446.

Linares, J.F., Duran, A., Reina-Campos, M., Aza-Blanc, P., Campos, A., Moscat, J., and Diaz-Meco, M.T. (2015). Amino acid activation of mTORC1 by a PB1-domain-driven kinase complex cascade. Cell Rep. *12*, 1339–1352.

Liu, Y. (2006). Fatty acid oxidation is a dominant bioenergetic pathway in prostate cancer. Prostate Cancer Prostatic Dis. *9*, 230–234.

MacInnis, R.J., and English, D.R. (2006). Body size and composition and prostate cancer risk: systematic review and meta-regression analysis. Cancer Causes Control *17*, 989–1003.

Moscat, J., Karin, M., and Diaz-Meco, M.T. (2016). p62 in cancer: signaling adaptor beyond autophagy. Cell *167*, 606–609.

Muller, T.D., Lee, S.J., Jastroch, M., Kabra, D., Stemmer, K., Aichler, M., Abplanalp, B., Ananthakrishnan, G., Bhardwaj, N., Collins, S., et al. (2013). p62 links beta-adrenergic input to mitochondrial function and thermogenesis. J. Clin. Invest. *123*, 469–478.

Nieman, K.M., Kenny, H.A., Penicka, C.V., Ladanyi, A., Buell-Gutbrod, R., Zillhardt, M.R., Romero, I.L., Carey, M.S., Mills, G.B., Hotamisligil, G.S., et al. (2011). Adipocytes promote ovarian cancer metastasis and provide energy for rapid tumor growth. Nat. Med. *17*, 1498–1503.

Olson, M.V., Lee, J., Zhang, F., Wang, A., and Dong, Z. (2006). Inducible nitric oxide synthase activity is essential for inhibition of prostatic tumor growth by interferon-beta gene therapy. Cancer Gene Ther. *13*, 676–685.

Ouchi, N., Parker, J.L., Lugus, J.J., and Walsh, K. (2011). Adipokines in inflammation and metabolic disease. Nat. Rev. Immunol. *11*, 85–97.

Park, E.J., Lee, J.H., Yu, G.Y., He, G., Ali, S.R., Holzer, R.G., Osterreicher, C.H., Takahashi, H., and Karin, M. (2010). Dietary and genetic obesity promote liver inflammation and tumorigenesis by enhancing IL-6 and TNF expression. Cell *140*, 197–208.

Petruzzelli, M., Schweiger, M., Schreiber, R., Campos-Olivas, R., Tsoli, M., Allen, J., Swarbrick, M., Rose-John, S., Rincon, M., Robertson, G., et al. (2014). A switch from white to brown fat increases energy expenditure in cancer-associated cachexia. Cell Metab. *20*, 433–447.

Rakhshandehroo, M., Knoch, B., Muller, M., and Kersten, S. (2010). Peroxisome proliferator-activated receptor alpha target genes. PPAR Res. *2010*, https://doi.org/10.1155/2010/612089.

Rangaswami, H., Bulbule, A., and Kundu, G.C. (2006). Osteopontin: role in cell signaling and cancer progression. Trends Cell Biol. *16*, 79–87.

Reina-Campos, M., Moscat, J., and Diaz-Meco, M. (2017). Metabolism shapes the tumor microenvironment. Curr. Opin. Cell Biol. *48*, 47–53.

Rodriguez, A., Duran, A., Selloum, M., Champy, M.F., Diez-Guerra, F.J., Flores, J.M., Serrano, M., Auwerx, J., Diaz-Meco, M.T., and Moscat, J. (2006). Mature-onset obesity and insulin resistance in mice deficient in the signaling adapter p62. Cell Metab. *3*, 211–222.

Rodriguez, C., Patel, A.V., Calle, E.E., Jacobs, E.J., Chao, A., and Thun, M.J. (2001). Body mass index, height, and prostate cancer mortality in two large cohorts of adult men in the United States. Cancer Epidemiol. Biomarkers Prev. *10*, 345–353.

Schlaepfer, I.R., Rider, L., Rodrigues, L.U., Gijon, M.A., Pac, C.T., Romero, L., Cimic, A., Sirintrapun, S.J., Glode, L.M., Eckel, R.H., and Cramer, S.D. (2014). Lipid catabolism via CPT1 as a therapeutic target for prostate cancer. Mol. Cancer Ther. *13*, 2361–2371.

Shevde, L.A., Das, S., Clark, D.W., and Samant, R.S. (2010). Osteopontin: an effector and an effect of tumor metastasis. Curr. Mol. Med. *10*, 71–81.

Sutcliffe, S., and Platz, E.A. (2007). Inflammation in the etiology of prostate cancer: an epidemiologic perspective. Urol. Oncol. *25*, 242–249.

Valencia, T., Kim, J.Y., Abu-Baker, S., Moscat-Pardos, J., Ahn, C.S., Reina-Campos, M., Duran, A., Castilla, E.A., Metallo, C.M., Diaz-Meco, M.T., and Moscat, J. (2014). Metabolic reprogramming of stromal fibroblasts through p62-mTORC1 signaling promotes inflammation and tumorigenesis. Cancer Cell *26*, 121–135.

Venkateswaran, V., Haddad, A.Q., Fleshner, N.E., Fan, R., Sugar, L.M., Nam, R., Klotz, L.H., and Pollak, M. (2007). Association of diet-induced hyperinsulinemia with accelerated growth of prostate cancer (LNCaP) xenografts. J. Natl. Cancer Inst. *99*, 1793–1800.

von Hafe, P., Pina, F., Perez, A., Tavares, M., and Barros, H. (2004). Visceral fat accumulation as a risk factor for prostate cancer. Obes. Res. *12*, 1930–1935.

Wolin, K.Y., Carson, K., and Colditz, G.A. (2010). Obesity and cancer. Oncologist *15*, 556–565.

Wright, M.E., Chang, S.C., Schatzkin, A., Albanes, D., Kipnis, V., Mouw, T., Hurwitz, P., Hollenbeck, A., and Leitzmann, M.F. (2007). Prospective study of adiposity and weight change in relation to prostate cancer incidence and mortality. Cancer *109*, 675–684.

STAR★METHODS

KEY RESOURCES TABLE

REAGENT or RESOURCE	SOURCE	IDENTIFIER
Antibodies		
Rabbit anti-phospho-4EBP1 (T37/46)	Cell Signaling	#2855; RRID: AB_560835
Rabbit anti-phosho-S6 (Ser240/244)	Cell Signaling	#5364; RRID: AB_10694233
Goat anti-OPN	R&D	AF808; RRID: AB_2194992
Rabbit anti-FASN	Abcam	ab22759; RRID: AB_732316
Mouse anti-CPT1A	Abcam	ab128568; RRID: AB_11141632
Mouse anti-β-actin	Sigma-Aldrich	A1978; RRID: AB_476692
Mouse anti-F4/80	eBioscience	14-4801-85; RRID: AB_467559
Mouse anti-F4/80, APC conjugated	eBioscience	17-4801-82; RRID: AB_469452
Rabbit anti-ki67	Thermo Fisher	RM-9106-R7; RRID: AB_149920
Rabbit anti cleaved caspase 3	Cell Signaling	# 9664; RRID: AB_2070042
Rabbit anti-SQSTM1/p62	Thermo Scientific	PA5-20839; RRID: AB_11157045
Rat anti-mouse IgG1, secondary	BD Biosciences	550331; RRID: AB_2296342
Donkey anti-goat IgG, Alexa fluor 568	Invitrogen	A-11057; RRID: AB_2534104
Goat anti-rabbit, secondary	Dako	E0432; RRID: AB_2313609
Rabbit anti-goat, secondary	Dako	E0466
Bacterial and Virus Strains		
Lentiviral packaging plasmid psPAX2	Addgene	#12260
Lentiviral packaging plasmid pMD2.G	Addgene	#12259
Lentiviral shRNA targeting mouse CPT1A	Sigma-Aldrich	TRCN0000305935 TRCN0000110599 TRCN0000110597
Chemicals, Peptides, and Recombinant Proteins		
Tyramine, Alexa fluor 488	Invitrogen	B40953
Recombinant mouse OPN	R&D	441-OP-200
Etomoxir	Sigma-Aldrich	E1905
Oligomycin	Sigma-Aldrich	75351
FCCP	Sigma-Aldrich	C2920
Antimycin A	Sigma-Aldrich	A8674
Rotenone	Sigma-Aldrich	R8875
Carnitine	Sigma-Aldrich	C0158
Advanced DMEM/F12	Gibco	12634010
Y-27632	Tocris	1254
B27 Supplement	Gibco	17504001
N2 Supplement	Gibco	17502048
Murine EGF	Thermo Fisher	PMG8045
Recombinant R-Spodin	R&D	3474-RS-050
Recombinant Noggin	Peprotech	250-38
A83-01 inhibitor	Tocris	2939

(Continued on next page)

REAGENT or RESOURCE	SOURCE	IDENTIFIER
Dihydrotestosterone	Sigma	A8380
Dexamethasone	Sigma-Aldrich	D1756
3-Isobutyl-1-methylxanthine (IBMX)	Sigma-Aldrich	I7018
Rosiglitazone	Sigma-Aldrich	R2408
X-tremeGENE transfection reagent	Roche	6366236001
Collagenase II	Sigma-Aldrich	C6885
Human insulin solution	Sigma-Aldrich	I9278
Matrigel basement membrane matrix	Corning	354234
Collagen type I	Corning	354236
Growth factor reduced Matrigel	Corning	356230
TrypLE	Gibco	12604013
Critical Commercial Assays		
Mouse Osteopontin/OPN ELISA assay	R&D	MOST00
Matrigel invasion assay	Corning	354480
Migration assay	Corning	354578
Triglyceride quantification assay	Wako	992-02892,998-02992
Cholesterol quantification assay	Wako	999-02601
M.O.M. kit	Vector	BMK-2202
VECTASTAIN® Elite® ABC-HRP Kit	Vector	PK-6100
Mouse APC Selection Kit	StemCell	18452
SeaHorse Seahorse XF24 Islet Capture FluxPak	Agilent	101174-100
Deposited Data		
RNAseq	GEO	GSE100060
Raw Data	This study; Mendeley Data	https://doi.org/10.17632/hzm74h2k3x.1
Experimental Models: Cell Lines		
Myc-CAP	Dr. Charles Sawyers	N/A
TRAMP C2RE3	(Olson et al., 2006)	N/A
SVF (WT and p62 KO)	This study	N/A
Experimental Models: Organisms/Strains		
p62 $_{global}$ KO	(Duran et al., 2004)	N/A
p62$^{f/f}$aP2-Cre (p62^{Adipo})	(Muller et al., 2013)	N/A
TRAMP^{+} hemizygous	(Greenberg et al., 1995)	N/A
Oligonucleotides		
Full sequences in Table S2	IDT	N/A
Software and Algorithms		
Image J	NIH	https://imagej.nih.gov/ij/
Adiposoft (Image J)	N/A	http://imagej.net/Adiposoft
ImageProPlus 6	MediaCybernetics	N/A
Graphpad Prism 7	Graphpad	https://www.graphpad.com/scientific-software/prism/
GenePattern	Broad Institute	https://genepattern.broadinstitute.org/gp/pages/index.jsf
GSEA v2.0.14	Broad Institute	http://www.broadinstitute.org/gsea/index.jsp
Morpheus	Broad Institute	https://software.broadinstitute.org/morpheus/
CIBERSORT	Stanford	https://cibersort.stanford.edu/
cBioportal	N/A	http://www.cbioportal.org/index.do
Oncomine	N/A	www.oncomine.org
SignalP 4.1	N/A	http://www.cbs.dtu.dk/services/SignalP/
UCSC Xena	UCSC	https://xenabrowser.net/datapages/

CONTACT FOR REAGENT AND RESOURCE SHARING

Further information and requests for resources and reagents should be directed to and will be fulfilled by the Lead Contact, Maria T Diaz-Meco (mdmeco@sbpdiscovery.org)

EXPERIMENTAL MODEL AND SUBJECT DETAILS

Mouse Models

WT and p62KO mice were previously described (Duran et al., 2004). p62$^{f/f}$Ap2-Cre mice were previously described (Muller et al., 2013). TRAMP$^+$ mice were previously described (Greenberg et al., 1995). All mouse strains were generated in a C57BL/6 background. All mice were born and maintained under pathogen-free conditions. All genotyping was done by PCR. Male mice were sacrificed and adipose tissues and genitourinary (GU) sections were dissected. Animal handling and experimental procedures were approved by the Institutional Animal Care and Use Committee at SBP Medical Discovery Institute.

Cell Lines

PCa cells (TRAMP-C2RE3 and Myc-CAP) are cultured in DMEM supplemented with 10% FBS. Knock down of CPT1A in PCa cells was achieved by mammalian Lentiviral shRNAs transduction. Briefly, lentiviral shRNA-encoding plasmids were cotransfected with packaging plasmids into actively growing HEK293T cells by using X-tremeGENE transfection reagent. Virus-containing supernatants were collected 48 hours after transfection, filtered to eliminate cells, and then used to infect target cells in the presence of 8 μg/ml polybrene. Cells were selected with puromycin (3 μg/ml). For primary adipocyte and stroma vascular fraction (SVF), epididymal adipose tissue was excised and minced in 10 ml of HBSS solution containing 0.5% BSA-Fatty acid free. Collagenase II (0.5 mg/ml) was added, and the tissue was incubated at 37°C with shaking (30 min). A total of 10 mM EDTA was added 5 min before the end of the incubation. Larger particles were removed using a 100 μm cell strainer, and the filtrates were centrifuged at 500 g for 5 min three times to separate floating adipocytes and pelleted stromal vascular fraction (SVF) and remove collagenase residue. SVF were suspended in erythrocyte lysis buffer (155 mM NH4Cl, 10 mM KHCO3, and 0.1 mM EDTA) and incubated at room temperature for 5 min to deplete erythrocytes. Adipocytes and SVF were collected and suspended in DMEM/F12 containing 10% FBS for experiments. Enrichment of F4/80$^+$ cells (macrophages) in SVF was performed by magnetic immunoaffinity with APC conjugated F4/80 antibody and APC positive selection kit. For adipocyte differentiation, SVF were isolated from inguinal adipose tissue as mentioned above. Isolated SVF were seeded in culture dish for 2 days to eliminate the unattached dead cell/white blood cell populations. SVF including adipogenic precursors were passed into 6-well plate for in vitro differentiation. Two days post confluence, differentiation was initiated by induction cocktail (DMEM/F12 containing 1μM Dexamethasone, 10μg/ml Insulin, 0.5mM IBMX and 10μM Rosiglitazone and 10% FBS) for 3 days, followed by maintenance cocktail (DMEM/F12 containing 10μg/ml Insulin and 10% FBS) for another 4 days. Media were then changed to normal growth media till the endpoint of experiments. All cells are incubated at 37°C, 5% CO$_2$ atmosphere. For prostate organoids, murine prostates were enzymatically digested with collagenase type II and subsequently with TrypLE. Cells were seeded in growth factor reduced Matrigel and overlaid with advanced DMEM/F12 medium containing: Glutamax, Hepes, Normocin, 1x B27, 1x N2, 50 ng/ml EGF, 500 ng/ml recombinant R-spondin1, 100 ng/ml recombinant Noggin, 200 nM TGF-β/Alk inhibitor and 1 nM Dihydrotestosterone.

METHOD DETAILS

Indirect Calorimetry

Food intake, drinking, heat production, energy expenditure, respiratory exchange ratio, and home-cage activity were assessed in male mice of 7-month-old using an automated indirect calorimetry Oxymax system of the Comprehensive Lab Animal Monitoring System (CLAMS; Columbus Instruments) at UCSD Animal Care Program. After 24 hr of adaptation, O$_2$ consumption and CO$_2$ production were measured every 13 min for a total of up to 72 hr to determine the respiratory quotient and energy expenditure. Food intake was determined continuously for the same time as the indirect calorimetry assessments by integration of scales into the sealed cage environment. Home-cage locomotor activity was determined using a multidimensional infrared light beam system with beams scanning the bottom and top levels of the cage, and activity being expressed as beam breaks.

Body Composition Measurements

Whole-body composition (fat and lean mass) in male mice of 7-month-old was measured using Dual-Energy X-ray Absorptiometry (DXA) at UCSD Animal Care Program.

Immunoblot Analysis

Protein extracts were separated by SDS-PAGE and transferred to Immobilon-P PVDF membranes (Millipore). After blocking with 5% nonfat dry milk in Tris-buffered saline and 0.1% Tween (TBS-T), the membranes were incubated with the indicated antibodies overnight at 4°C. After 2 hr incubation with the appropriate horseradish peroxidase-conjugated antibodies, the immune complexes were detected by chemiluminescence (Thermo Scientific).

Histological Analysis

Tissues from indicated male mice were isolated, rinsed in ice-cold PBS, fixed in 10% neutral buffered formalin for 24 h, dehydrated, and embedded in paraffin. Livers were embedded in Tissue Tek O.C.T. compound and snap frozen in dry ice, then kept in -80 °C. Tissue sections (5 μm) were stained with hematoxylin and eosin (H&E). Pathological characterization of cancer sample degree was assessed using the reported criteria (Ittmann et al., 2013) in a blinded fashion by a pathologist. Histological sections of epidydimal fat pads were stained with H&E and studied under 20-fold magnification to compare adipocyte size. At least seven fields per section from four different mice of each genotype were randomly selected to determine the adipocyte size and number according to morphological feature using "ImageJ"-based software "Adiposoft". Frozen liver sections (5 μm) were stained with Oil red O (Sigma-Aldrich) to detect lipid accumulation. Sections were fixed in paraformaldehyde and stained for 3 h in 0.5% Oil red O in propylene glycol, followed by 1 min incubations in 85% aqueous propylene glycol. After the slides were washed in distilled water, they were counterstained with Harris's hematoxylin for 10s. For immunohistochemical (IHC) detection, sections were deparaffinized, rehydrated, and treated for antigen retrieval. After blocking with Avidin/Biotin blocking kit or M.O.M. Ig Blocking Reagent, tissues were incubated with primary antibody overnight at 4°C (OPN) or 30 min at room temperature (F4/80) followed by incubation with biotinylated secondary antibody. Endogenous peroxidase was quenched in 3% H_2O_2 in water for 10 min at room temperature. Antibodies were visualized with avidin/biotin complex Vectastain Elite using diaminobenzidine as the chromagen. For immunofluorescence, sections were incubated with Alexa-conjugated secondary antibodies (Life Technologies) and the samples examined with a Zeiss LSM 710 NLO Confocal Microscope.

Lipid Analysis

Plasma/tissue triglyceride and total cholesterol were determined spectrophotometrically (Wako Diagnostics, USA). For determination of lipids mass, liver sample were washed with PBS and frozen. Total lipids were isolated from homogenates by Folch extraction. Briefly, around 100 mg tissue samples were homogenized in 1 mL methanol, homogenates were further mixed with 2 ml chloroform and rotated mildly for 2 hr to extract lipid. Samples were then mixed roughly with 1 ml H_2O for 30 s to separate phases. The lipid-containing organic phase (bottom) were collected and dried by nitrogen. Total lipids were dissolved in PBS containing 1% Triton-X 100, followed by quantification by kits. The tissue lipid concentrations were normalized to tissue protein mass.

Adipose Tissue Conditioned Media

1g epididymal adipose tissue were minced thoroughly and incubated in 4 ml serum-free DMEM containing 1% BSA-Fatty acid free for 24 h. Conditioned media were aliquoted and frozen in -80°C until use.

Migration and Invasion Assay

Wildtype, shNT and shCPT1A PCa cells (TRAMP-C2RE3 and Myc-CAP) were assayed for their ability to migrate or invade through a polyethylene terephthalate membrane inserts in 24- well format using Corning BioCoat™ Insert System (Corning). A total of 2.5×10^4 cells/well were seeded into the inner chamber in serum-free DMEM, and cells were challenged with OPN (5 μg/ml in 0.2% FBS containing DMEM) or conditioned media of epidydimal WAT (WT and p62 KO mice) in the outer chamber. After indicated incubation at 37°C, 5% CO_2, cells that migrated/invaded through the pores onto the bottom of the insert were fixed in 100% methanol and stained with crystal violet. The total number of migrating/invading cells was determined by counting the cells on the lower surface of the insert using a light microscope at 20x magnification.

RNA Analysis

Total RNA from mouse tissues and cultured cells was isolated using the TRIZOL reagent (Invitrogen) and the RNeasy Mini Kit (QIAGEN), followed by DNase treatment. After quantification using a Nanodrop 1000 spectrophotometer (Thermo Scientific), RNA was reverse-transcribed using random primers and MultiScribe Reverse Transcriptase (Applied Biosystems). Gene expression was analyzed by amplifying 20 ng of the complementary DNA using the CFX96 Real Time PCR Detection System with SYBR Green Master Mix (BioRad) and primers described in Table S2. The amplification parameters were set at 95°C for 30 s, 58°C for 30 s, and 72°C for 30 s (40 cycles total). Gene expression values for each sample were normalized to the 18S RNA.

Organotypic Cultures

3D air liquid organotypic culture set up as previously described (Valencia et al., 2014), has been used to determine the mechanisms of prostate cancer cell invasion and the role of the adipose tissue compartments on cancer cell invasion. Briefly, gels were composed of 1.75 volumes of Matrigel, 5.25 volumes of collagen type I, 1 volume of 1x DMEM, 1 volume of 10x DMEM, and 1 volume of filtered FBS. 0.9 ml gels were then mixed with 0.1 ml cell suspension containing 300,000 adipocytes, 1,000,000 SVF cells or 40 mg minced WAT. The cell-gel/tissue-gel mixture was plated onto 24-well plates coated with diluted collagen type I. Gels were equilibrated with 1 ml of 1x DMEM overnight at 37°C. 5×10^5 cells PCa cells were then seeded on top of the matrix. Gel rafts were placed onto collagen-coated nylon sheets and lifted using a sterile supporting steel mesh to set up a raised air-liquid culture. Normal medium was changed in alternate days and organotypic cultures were maintained to grow for 14 days. Afterwards, organotypic gels were harvested, fixed in

10% neutral buffered formalin, bisected and embedded in paraffin. H&E stained sections were analyzed with a Zeiss light microscope supplemented with Axiovision40 software. Quantification of the invasion assays was performed using ImageProPlus software.

Respiration Assays

The cellular oxygen consumption rate (OCR) of primary adipocytes was determined using an XFp Extracellular Flux Analyzer (Seahorse Bioscience). Prior to assay, 10,000 WT and p62 KO SVF cells were seeded into XFp microplates. One day later, Adipogenic differentiation was initiated using a protocol mentioned above. Seven days post differentiation, adipocyte culture medium was changed to XF basal medium containing 10 mM glucose, and 1 mM pyruvate. The uncoupled and maximal OCRs were determined using 1 μM oligomycin and 1 μM FCCP (carbonyl cyanide p-trifluoromethoxyphenylhydrazone), respectively. Complex-I-dependent respiration was inhibited with a mix of antimycin A and rotenone, 2 μM each. Oxygen consumption values were normalized to protein content. OCR of intact adipose tissue explants was measured using a XF24 Extracellular Flux Analyzer (Seahorse Bioscience). Briefly, freshly isolated inguinal adipose tissues were harvested from 7-month-old mice and was rinsed with unbuffered DMEM (pH 7.4). The adipose tissue was cut into sections using a 2mm biopsy punch, and 2 punches were placed in each well of an XF24 Islet Capture Microplate (Seahorse Bioscience). The tissue was then covered with a screen, which allowed free perfusion while minimizing tissue movement. XF basal medium supplemented with 10 mM glucose and 1 mM pyruvate was then added to each well. At least 4 to 6 replicates from each animal were used for the assay. The plate was incubated at 37°C in a non-CO2 incubator for 30 minutes before extracellular flux analysis. After five baseline measurements, OCR was measured after the addition of the following drugs: 10 μM oligomycin, 20 μM FCCP, and 12 μM rotenone + 12 μM antimycin A as indicated. Oxygen consumption values were normalized to protein content. The oxygen consumption rate of prostate organoids was measured using a XF24 Extracellular Flux Analyzer (Seahorse Bioscience). Organoids were prepared from prostates of 2-month-old TRAMP$^+$ hemizygous mice and treated with 3 μg/ml OPN for 5 days, starting 2 days after seeding. OPN was refreshed every two days. After 5 days of OPN treatment, organoids were harvested using cold PBS and seeded in XF medium with 10 mM glucose, 0.5 mM carnitine and 5 mM Hepes on top of a matrigel-precoated XF24 microplate. The plate was centrifuged at 600g for 5 min, and then incubated at 37°C in a non-CO2 incubator for 30 minutes before extracellular flux analysis. After five baseline measurements, OCR was measured after the addition of the following drugs: 15 μM oligomycin, 20 μM fluoro-carbonyl cyanide phenylhydrazone (FCCP), 200 μM etomoxir, and 12 μM rotenone + 12 μM antimycin A, as indicated.

RNAseq, Gene Set Enrichment Analysis, CIBERSORT and Secretome Analysis

The gene matrix files of adipose tissues and prostate tumors of TRAMP$^+$/p62^{Adipo} and TRAMP$^+$/WT mice were generated with RNAexpress app (Illumina) and compared using T-test comparison and log2 ratio of classes. Raw gene expression data from relevant datasets were directly accessed through the GEO (https://www.ncbi.nlm.nih.gov/geo/). GenePattern (https://genepattern.broadinstitute.org/gp/pages/index.jsf) was used to collapse gene matrix files (CollapseDataset module) or to assess the statistical significance of differential gene expression (ComparativeMarkerSelection module for microarray data and DESeq2 module for RNAseq data). Gene Set Enrichment Analysis (GSEA) was performed using GSEA v2.0.14 software (http://www.broadinstitute.org/gsea/index.jsp) with 1000 gene-set permutations using the gene-ranking metric T-test with the collections H.all.V5.2.symbols (Hallmarks), c5.all.v6.1.symbols (C5) or customized signatures. The "PPARA TRAGET GENES" signature was generated based on a list of PPARα target genes (size = 156, Table S1) that are reportedly regulated by PPARα in the context of fatty acid and glucose metabolism (Rakhshandehroo et al., 2010). The "WAT_RAPAMYCIN_UP" (size = 165) and "WAT_RAPAMYCIN_DN" (size = 261) signatures were generated based on differential expressed genes (p < 0.01) in WAT from Rapamycin-treated mice (GSE52825). The "PRAD_SPP1" signature was created by computing Pearson correlation coefficients of *SPP1* with every gene in TCGA PRAD dataset. Top 159 most correlated genes (r > 0.4, p < 0.05) was used as the signature. Heat-map representation of gene expression was generated using Morpheus (https://software.broadinstitute.org/morpheus/). The abundances of immune cell types in WAT were estimated by CIBERSORT (https://cibersort.stanford.edu/) using RNAseq expression data. For WAT secretome analysis, differentially expressed gene candidates (Log2 FC > 1.5 or < -1.5, FDR q < 0.05) analyzed by RNAseq were subjected to SignalP 4.1 (http://www.cbs.dtu.dk/services/SignalP/) to estimate the present of secretion signal peptide. The predicted candidates were ranked based on fold change.

Bioinformatic Analysis of Clinical Data

Prostate cancer datasets were either obtained by cBioportal (http://www.cbioportal.org/index.do),GEO, Oncomine (www.oncomine.org) or from The Cancer Genome Atlas (TCGA) database through the tool UCSC Xena (https://xenabrowser.net/datapages/). Expression levels extracted from Oncomine were assessed by calculating the mean values of different probes wherever multiple probes were used to target the same gene. Values obtained from UCSC Xena was Pan-cancer normalized. Differential expressions of *SPP1* and FAO genes were assessed by Mann-Whitney U-test. Biochemical recurrence-free survival plots of patients with prostate adenocarcinoma (PRAD) were obtained from TCGA.

QUANTIFICATION AND STATISTICAL ANALYSIS

Statistical analysis was performed using GraphPad Prism 7. Unpaired Student's two-tailed t test and nonparametric Mann-Whitney test were used to determine significance of differences between groups where appropriate. Correlation was studied by Pearson's correlation test as indicated. Differences in Kaplan Meier plots was analyzed by Log-Rank test. Values of $p < 0.05$ were considered as significantly different.

DATA AND SOFTWARE AVAILABILITY

The accession number for the RNA-seq data reported in this paper is GSE100060. Unprocessed original data have been deposited to Mendeley Data and are available at https://doi.org/10.17632/hzm74h2k3x.1